Electronic Supplementary Material (ESI) for Chemical Science.

An Expeditive and Green Chemo-Enzymatic Route To Diester Sinapoyl-L-Malate Analogues: Sustainable Bioinspired And Biosourced UV Filters and Molecular Heaters

Benjamin Rioux,[§a] Louis M. M. Mouterde,[§a] Jimmy Alarcan,[§b] Temitope T. Abiola,[§c,d] Matthias J.A. Vink,[§e] Jack M. Woolley,[§c] Aurélien A. M. Peru,[a] Matthieu M. Mention,[a] Fanny Brunissen,[a] Giel Berden,[e] Jos Oomens,[e*] Albert Braeuning,[b*] Vasilios G. Stavros,[c,f*] and Florent Allais[a*]

[a] URD Agro-Biotechnologies Industrielles (ABI), CEBB, AgroParisTech, 51110, Pomacle, France.
Email: florent.allais@agroparistech.fr
[b] Department of Food Safety, German Federal Institute for Risk Assessment, Max-Dohrn-Str. 8-10, 10589, Berlin, Germany.
Email: albert.braeuning@bfr.bund.de
[c] Department of Chemistry, University of Warwick, Gibbet Hill Road, CV4 7AL, Coventry, United-Kingdom.
Email: v.stavros@warwick.ac.uk
[d] Department of Chemistry, Lash Miller Chemical Laboratories, 80 St. George Street, Toronto, ON, M5S 3H6.
[e] Radboud University, Institute for Molecules and Materials, FELIX Laboratory, Toernooiveld 7, 6525ED, Nijmegen, the Netherlands
Email: j.oomens@science.ru.nl
[f] School of Chemistry, University of Birmingham, Edgbaston, Birmingham B15 2TT, UK
Email: v.stavros@bham.ac.uk

[§] these authors contributed equally to this work

Electronic Supporting Information

Table of ContentsS

General Characterization data

Diethyl sinapoyl-L-malate

Pale yellow oil (83%); **UV:** λ_{max} (EtOH, nm) 334, ε (L.mol^{-1}.cm^{-1}) 20482. $[\alpha]_D^{25}$: +11 (C (g.mL^{-1}) 0.02, MeOH, 25.2 °C). **^{1}H NMR** (300 MHz, 25 °C, acetone-d_6) δ: 7.84 (1H, s, H-9), 7.64 (1H, d, *J* = 15.9 Hz, H-3), 7.06 (2H, s, H-5), 6.47 (1H, d, *J* = 15.8 Hz, H-2), 5.50 (1H, dd, *J* = 4.7 and 8.0 Hz, H-11), 4.17 (4H, m, H-13 and H-13'), 3.90 (6H, s, H-8), 2.95 (2H, m, H-12), 1.24 (6H, t, *J* = 7.1 Hz, H-15 and H-15'). **^{13}C NMR** (75 MHz, 25 °C, acetone-d_6) δ: 169.8 (C-10), 169.6 (C-13), 166.6 (C-1), 148.9 (C-6), 147.5 (C-3), 139.8 (C-7), 125.9 (C-4), 114.8 (C-2), 107.0 (C-5), 69.2 (C-11), 62.0 and 61.4 (C-14 and C-14'), 56.7 (C-8), 36.9 (C-12), 14.4 (C-15 and C-15'). **TOF MS ES+**: $[M+H]^+$ for $C_{19}H_{25}O_9$: *m/z* 397.1499; found: *m/z* 397.1498.

Dibutyl sinapoyl-L-malate

Pale yellow oil (83%); **UV:** λ_{max} (EtOH, nm) 334, ε (L.mol^{-1}.cm^{-1}) 22063. $[\alpha]_D^{25}$: +11 (C (g.mL^{-1}) 0.02, MeOH, 25.0 °C). **^{1}H NMR** (300 MHz, 25 °C, acetone-d_6) δ: 7.64 (1H, d, *J* = 15.8 Hz, H-3), 7.06 (2H, s, H-5), 6.47 (1H, d, *J* = 15.9 Hz, H-2), 5.52 (1H, dd, *J* = 4.7 and 8.0 Hz, H-11), 4.14 (4H, m, H-14 and H-14'), 3.90 (6H, s, H-8), 2.96 (2H, ABX system, J_{AX} = 4.7 Hz, J_{BX} = 8.0 Hz, H-12), 1.61 (4H, m, H-15 and H-15'), 1.39 (4H, hex, *J* = 7.6 Hz, H-16 and H-16'), 0.91 (6H, t, *J* = 7.3 Hz, H-17 and H-17'). **^{13}C NMR** (75 MHz, 25 °C, acetone-d_6) δ: 169.8 (C-10), 169.6 (C-13), 166.5 (C-1), 148.9 (C-6), 147.5 (C-3), 139.8 (C-7), 125.9 (C-4), 114.8 (C-2), 107.0 (C-5), 69.3 (C-11), 65.8 and 65.2 (C-14 and C-14'), 56.7 (C-8), 36.9 (C-12), 31.4 and 31.3 (C-15 and C-15'), 19.7 and 19.7 (C-16 and C-16'), 14.0 and 13.9 (C-17 and C-17'). **TOF MS ES+**: $[M+H]^+$ for $C_{23}H_{33}O_9$: *m/z* 453.2125; found: *m/z* 453.2120.

Dioctyl sinapoyl-L-malate

Pale yellow oil (95%); **UV:** λ_{max} (EtOH, nm) 336, ε (L.mol^{-1}.cm^{-1}) 20765. $[\alpha]_D^{25}$: +10 (C (g.mL^{-1}) 0.02, MeOH, 24.9 °C). **^{1}H NMR** (300 MHz, 25 °C, DMSO-d_6) δ: 9.04 (1H, s, H-9), 7.59 (1H, d, *J* = 15.8 Hz, H-3), 7.05 (2H, s, H-5), 6.59 (1H, d, *J* = 15.8 Hz, H-2), 5.43 (1H, dd, *J* = 4.9 and 7.4 Hz, H-11), 4.08 (4H, m, H-14 and H-14'), 3.80 (6H, s, H-8), 2.96 (2H, m, H-12), 1.55 (4H, m, H-15 and H-15'), 1.20 (20H, m, H-16 to H-20 and H-16' to H-20'), 0.81 (6H, t, *J* = 7.3 Hz, H-21 and H-21'). **^{13}C NMR** (75 MHz, 25 °C, DMSO-d_6) δ: 169.0 (C-10), 168.7 (C-13), 165.7 (C-1), 148.0 (C-6), 146.9 (C-3), 138.7 (C-7), 124.1 (C-4), 113.5 (C-2), 106.4 (C-5), 68.1 (C-11), 65.2 and 64.6 (C-14 and C-14'), 56.1 (C-8), 35.9 (C-12), 31.3 – 22.1 (C-16 to C-20 and C-16' to C-20'), 28.1 and 28.0 (C-15 and C-15'), 13.9 (C-21 and C-21'). **TOF MS ES+**: $[M+H]^+$ for $C_{31}H_{49}O_9$: *m/z* 565.3377; found: *m/z* 565.3377.

Dilauryl sinapoyl-L-malate

Pale yellow oil (99%); **UV:** λ_{max} (EtOH, nm) 335, ε (L.mol^{-1}.cm^{-1}) 22184. $[\alpha]_D^{25}$: +9.5 (C (g.mL^{-1}) 0.02, MeOH, 25.0 °C). **^{1}H NMR** (300 MHz, 25 °C, acetone-d_6) δ: 7.64 (1H, d, *J* = 15.9 Hz, H-3), 7.06 (2H, s, H-5), 6.48 (1H, d, *J* = 15.9 Hz, H-2), 5.52 (1H, dd, *J* = 4.7 and 7.9 Hz, H-11), 4.14 (4H, m, H-14 and H-14'), 3.90 (6H, s, H-8), 2.97 (2H, ABX system, J_{AX} = 4.7 Hz, J_{BX} = 8.0 Hz, H-12), 1.64 (4H, m, H-15 and H-15'), 1.27 (36H, m, H-16 to H-24 and H-16' to H-24'), 0.87 (6H, t, *J* = 7.3 Hz, H-25 and H-25'). **^{13}C NMR** (75 MHz, 25 °C, DMSO-d_6) δ: 168.9 (C-10), 168.6 (C-13), 165.7 (C-1), 148.0 (C-6), 146.9 (C-3), 138.8 (C-7), 124.1 (C-4), 113.4 (C-2), 106.4 (C-5), 68.1 (C-11), 65.1 and 64.5 (C-14 and C-14'), 56.1 (C-8), 35.9 (C-12), 31.3 (C-23 and C-23'), 29.1 – 28.7 (C-17 to C-22 and C-17' to C-22'), 28.1 and 28.0 (C-15 and C-15'), 25.4 and 25.3 (C-16 and C-16'), 22.1 (C-24 and C-24'), 13.9 (C-25 and C-25'). **TOF MS ES+**: $[M+H]^+$ for $C_{39}H_{65}O_9$: *m/z* 677.4629; found: *m/z* 677.4630.

Dicitronellyl sinapoyl-L-malate

Pale yellow oil (97%); **UV:** λ_{max} (EtOH, nm) 336, ε (L.mol^{-1}.cm^{-1}) 19776. $[\alpha]_D^{25}$: +3.5 (C (g.mL^{-1}) 0.02, MeOH, 25.4 °C). **^{1}H NMR** (300 MHz, 25 °C, $CDCl_3$) δ: 7.64 (1H, d, *J* = 15.9 Hz, H-3), 6.77 (2H, s, H-5), 6.36

(1H, d, *J* = 15.8 Hz, H-2), 5.80 (1H, s, H-9), 5.59 (1H, t, *J* = 6.1 Hz, H-11), 5.06 (2H, m, H-19 and H-19'), 4.19 (4H, m, H-14 and H-14'), 3.91 (6H, s, H-8), 2.94 (2H, d, *J* = 6.2 Hz, H-12), 1.95 (4H, hept, *J* = 7.9 Hz, H-18 and H-18'), 1.66 and 1.57 (12H, 2 s, H-21 and H-21', and H-22 and H-22'), 1.54 – 1.10 (10H, m, H-15 to H-17 and H-15' to H-17'), 0.90 and 0.88 (6H, 2 s, H-23 and H-23'). **^{13}C NMR** (75 MHz, 25 °C, $CDCl_3$) δ: 169.5 (C-10), 169.3 (C-13), 166.0 (C-1), 148.0 (C-6), 146.7 (C-3), 137.4 (C-7), 131.6 (C-20 and C-20'), 125.8 (C-4), 124.6 (C-19 and C-19'), 114.6 (C-2), 105.3 (C-5), 68.5 (C-11), 64.5 and 63.9 (C-14 and C-14'), 56.4 (C-8), 37.1 and 37.0 (C-17 and C-17'), 36.6 (C-12), 35.4 and 35.4 (C-15 and C-15'), 29.5 (C-16 and C-16'), 25.8 (C-21 and C-21'), 25.5 and 25.5 (C-18 and C-18'), 19.5 and 19.4 (C-23 and C-23'), 17.8 (C-22 and C-22'). **TOF MS ES+**: $[M+H]^+$ for $C_{35}H_{53}O_9$: *m/z* 617.3690; found: *m/z* 617.3692.

Digeranyl sinapoyl-L-malate

Pale yellow oil (91%); **UV:** λ_{max} (EtOH, nm) 335, ε (L.mol^{-1}.cm^{-1}) 20555. $[\alpha]_D^{25}$: +4 (C (g.mL^{-1}) 0.02, MeOH, 25.5 °C). **^{1}H NMR** (300 MHz, 25 °C, DMSO-d_6) δ: 7.59 (1H, d, *J* = 15.8 Hz, H-3), 7.05 (2H, s, H-5), 6.58 (1H, d, *J* = 15.8 Hz, H-2), 5.42 (1H, m, H-11), 5.27 (2H, t, *J* = 7.1 Hz, H-15 and H-15'), 5.02 (2H, m, H-19 and H-19'), 4.60 (4H, m, H-14 and H-14'), 3.79 (6H, s, H-8), 2.94 (2H, ABX system, J_{AX} = 5.0 Hz, J_{BX} = 7.5 Hz, H-12), 2.00 (8H, m, H-17, H-18, H-17' and H-18'), 1.64 to 1.57 (12H, m, H-21, H-22, H-21' and H-22'), 1.54 and 1.52 (6H, 2s, H-23 and H-23'). **^{13}C NMR** (75 MHz, 25 °C, $CDCl_3$) δ: 169.0 (C-10), 168.6 (C-13), 165.7 (C-1), 148.1 (C-6), 147.0 (C-3), 142.3 and 141.9 (C-16 and C-16'), 138.7 (C-7), 131.2 and 131.1 (C-20 and C-20'), 124.2 (C-4), 124.0 (C-19 and C-19'), 118.1 and 117.8 (C-15 and C-15'), 113.5 (C-2), 106.5 (C-5), 68.1 (C-11), 61.9 and 61.3 (C-14 and C-14'), 56.1 (C-8), 38.7 (C-17 and C-17'), 35.9 (C-12), 25.8 and 25.8 (C-18 and C-18'), 25.5 (C-21 and C-21'), 17.6 and 17.5 (C-22 and C-22'), 16.2 (C-23 and C-23'). **TOF MS ES+**: $[M+H]^+$ for $C_{35}H_{49}O_9$: *m/z* 613.3377; found: *m/z* 613.3377.

Difarnesyl sinapoyl-L-malate

Pale yellow oil (94%); **UV:** λ_{max} (EtOH, nm) 336, ε (L.mol^{-1}.cm^{-1}) 21254. $[\alpha]_D^{25}$: +2 (C (g.mL^{-1}) 0.02, MeOH, 24.9 °C). **^{1}H NMR** (300 MHz, 25 °C, $CDCl_3$) δ: 7.64 (1H, d, *J* = 15.9 Hz, H-3), 6.77 (2H, s, H-5), 6.36 (1H, d, *J* = 15.8 Hz, H-2), 5.79 (1H, s, H-9), 5.61 (1H, t, *J* = 6.2 Hz, H-11), 5.33 (2H, m, H-15 and 15'), 5.08 (4H, m, H-19, H-23, H-19' and H-23'), 4.67 (4H, m, H-14 and H-14'), 3.91 (6H, s, H-8), 2.95 (2H, d, *J* = 6.2 Hz, H-12), 2.13-1.95 (16H, m, H-17, H-18, H-21, H-22, H-17', H-18', H-21', and H-22'), 1.69 and 1.59 (24H, 3 s, H-25, H-26, H-27, H-28, H-25', H-26', H-27' and H-28'). **^{13}C NMR** (75 MHz, 25 °C, $CDCl_3$) δ: 169.4 (C-10), 169.2 (C-13), 166.0 (C-1), 147.3 (C-6), 146.6 (C-3), 143.4 143.3 143.0 143.0 (C-16 and C-16' *mixture of isomers*), 137.5 (C-7), 135.8 135.8 135.7 and 135.6 (C-20 and C-20' *mixture of isomers*), 131.7 and 131.5 (C-24 and C-24'), 125.9 (C-4), 124.4 (C-23 and C-23'), 123.7 and 123.6 (C-15 and C-15'), 117.9 and 117.7 (C-19 and C-19'), 114.7 (C-2), 106.4 (C-5), 68.5 (C-11), 62.3 and 62.1 (C-14 and C-14'), 56.4 (C-8), 40.0 39.8 39.7 and 37.0 (C-17 and C-17' *mixture of isomers*), 36.6 (C-12), 26.8 26.7 26.4 and 26.2 (C-18, C-21, C-22, C-18', C-21' and C-22'), 25.8 and 23.5 (C-28 and C-28'), 17.8 16.6 and 16.1 (C-25, C-26, C-27, C-25', C-26' and C-27'). **TOF MS ES+**: $[M+H]^+$ for $C_{45}H_{65}O_9$: *m/z* 749.4629; found: *m/z* 749.4629.

Dioleylyl sinapoyl-L-malate

Pale yellow oil (88%); **UV:** λ_{max} (EtOH, nm) 336, ε (L.mol^{-1}.cm^{-1}) 19091. $[\alpha]_D^{25}$: +4 (C (g.mL^{-1}) 0.02, EtOH, 24.7 °C). **^{1}H NMR** (300 MHz, 25 °C, $CDCl_3$) δ: 7.65 (1H, d, *J* = 15.9 Hz, H-3), 6.77 (2H, s, H-5), 6.36 (1H, d, *J* = 15.9 Hz, H-2), 5.79 (1H, s, H-9), 5.60 (1H, t, *J* = 6.1 Hz, H-11), 5.33 (4H, m, H-22, H-23, H-22' and H-23'), 4.14 (4H, m, H-14 and H-14'), 3.92 (6H, s, H-8), 2.95 (2H, m, H-12), 2.00 (8H, m H-21, H-24, H-21' and H-24'), 1.63 (4H, m, H-15 and H-15'), 1.38 – 1.19 (44H, m, H-16 to H-20, H-25 to H-30, H-16' to H-20' and H-25' to H-30'), 0.87 (6H, t, *J* = 6.5 Hz, H-31 and H-31'). **^{13}C NMR** (75 MHz, 25 °C, $CDCl_3$) δ: 169.5 (C-10), 169.3 (C-13), 166.0 (C-1), 147.3 (C-6), 146.7 (C-3), 137.5 (C-7), 130.1 and 129.9 (C-22, C-23, C-22' and C-23'), 125.8 (C-4), 114.7 (C-2), 105.3 (C-5), 68.5 (C-11), 66.1 and 65.5 (C-14 and C-14'), 56.4

(C-8), 36.6 (C-12), 32.0 (C-29 and C-29'), 29.9 – 29.3 (C-17 to C-20, C-25 to C-28, C-17' to C-20' and C-25' to C-28'), 28.7 and 28.6 (C-15 and C-15'), 27.3 and 27.3 (C-21, C-24, C-21' and C-24'), 26.0 and 25.9 (C-16 and C-16'), 22.8 (C-30 and C-30'), 14.3 (C-31 and C-31'). **TOF MS ES+**: $[M+H]^+$ for $C_{51}H_{85}O_9$: *m/z* 841.6194; found: *m/z* 841.6197.

NMR spectra of diester sinapoyl-L-malate series

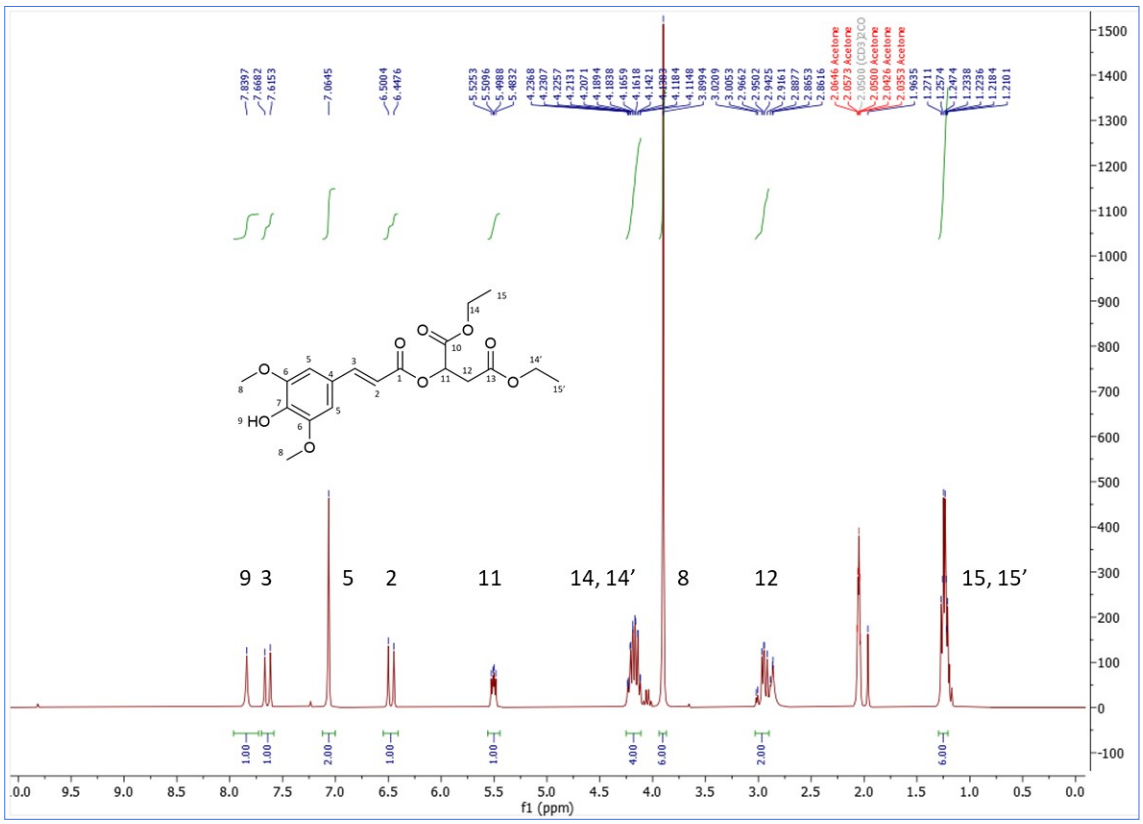

Figure S1: ^{1}H spectrum of diethyl sinapoyl-L-malate.

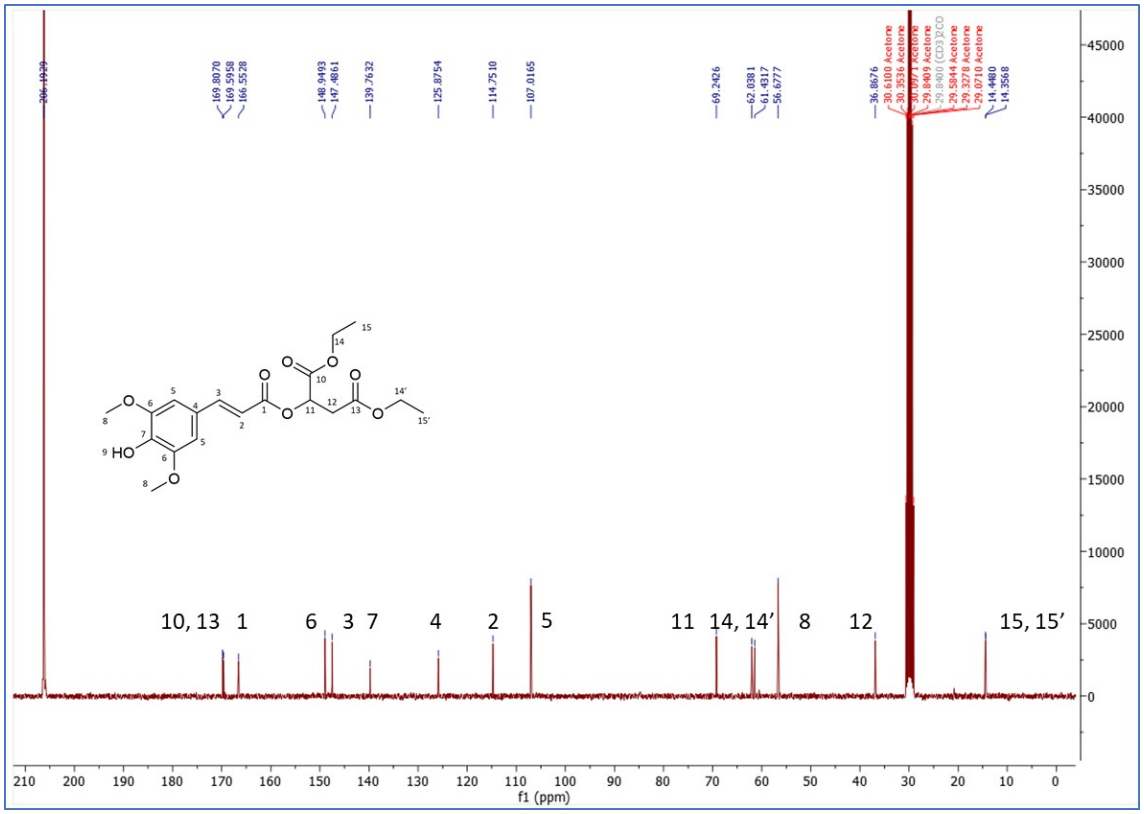

Figure S2: ^{13}C spectrum of diethyl sinapoyl-L-malate.

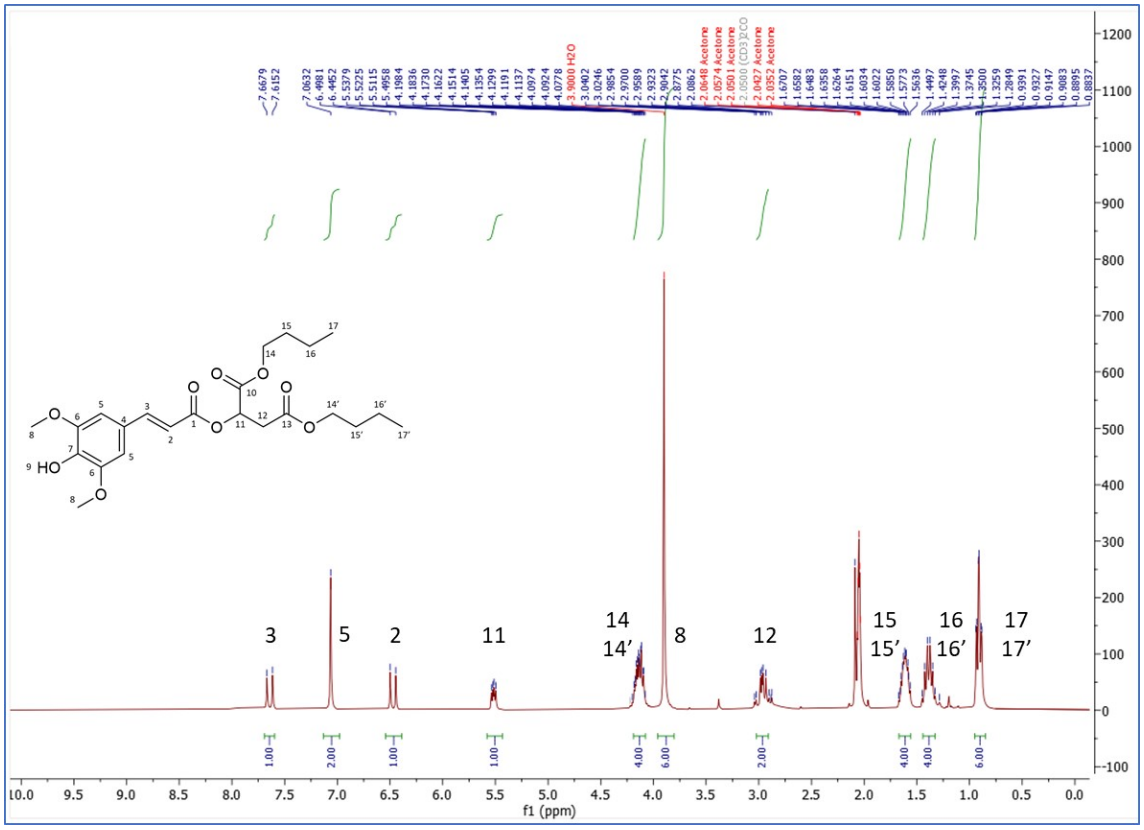

Figure S3: ^{1}H spectrum of dibutyl sinapoyl-L-malate.

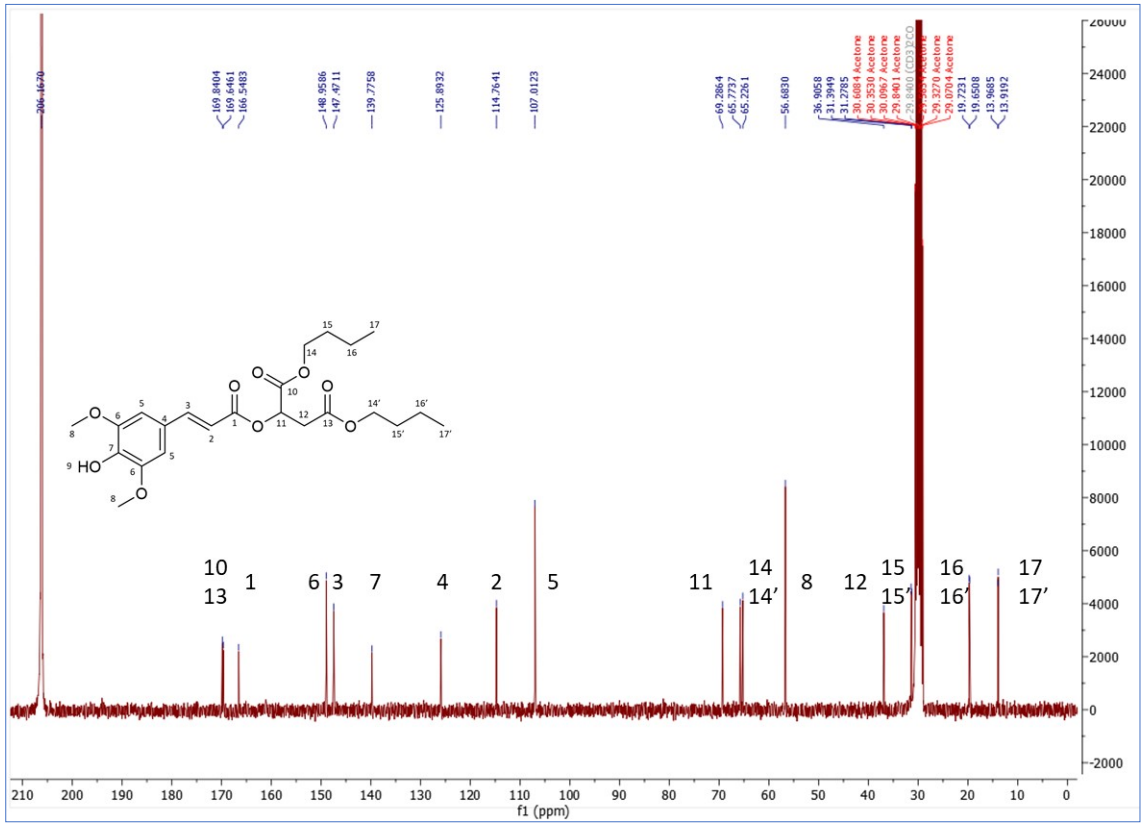

Figure S4: ^{13}C spectrum of dibutyl sinapoyl-L-malate.

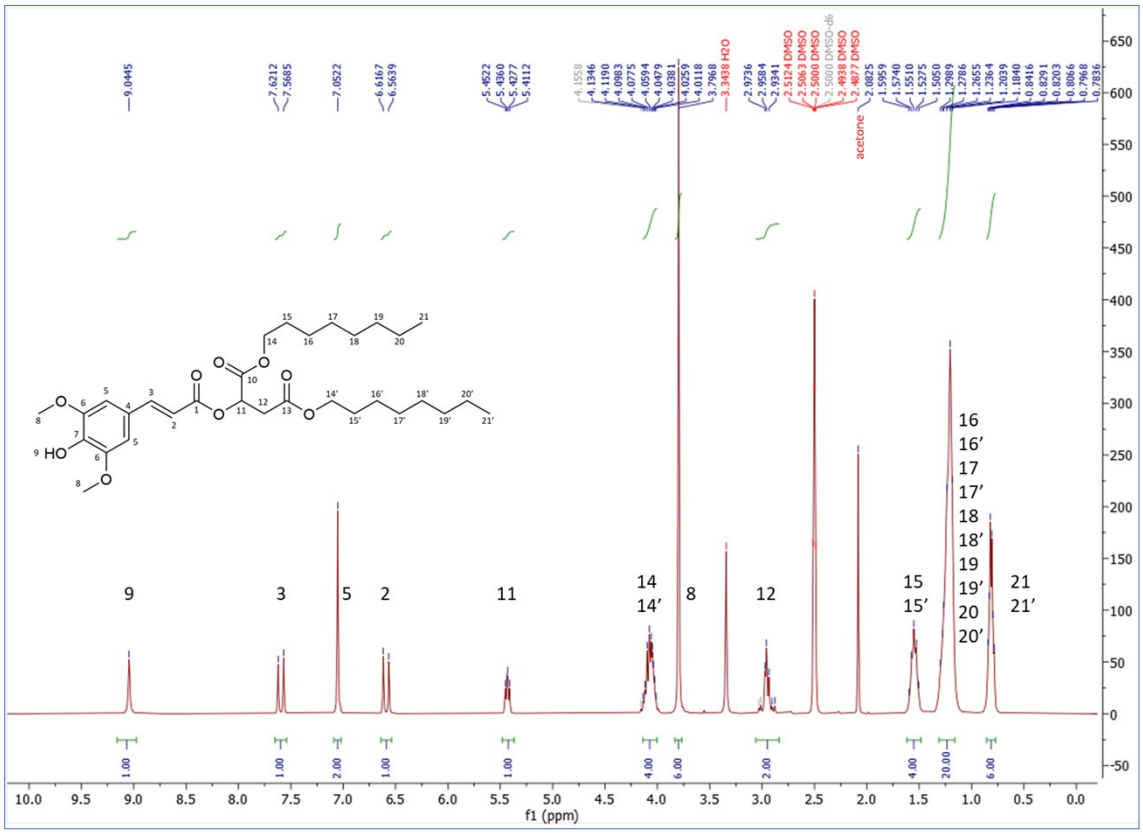

Figure S5: ^{1}H spectrum of dioctyl sinapoyl-L-malate.

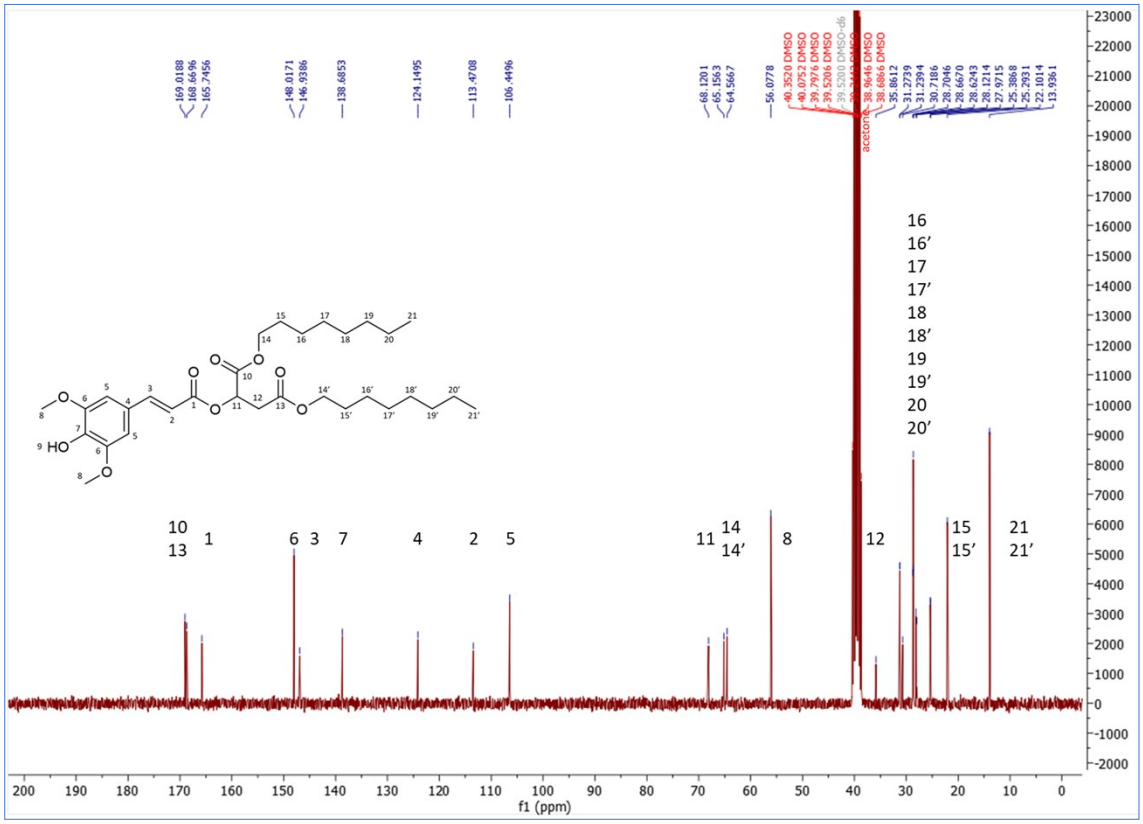

Figure S6: ^{13}C spectrum of dioctyl sinapoyl-L-malate.

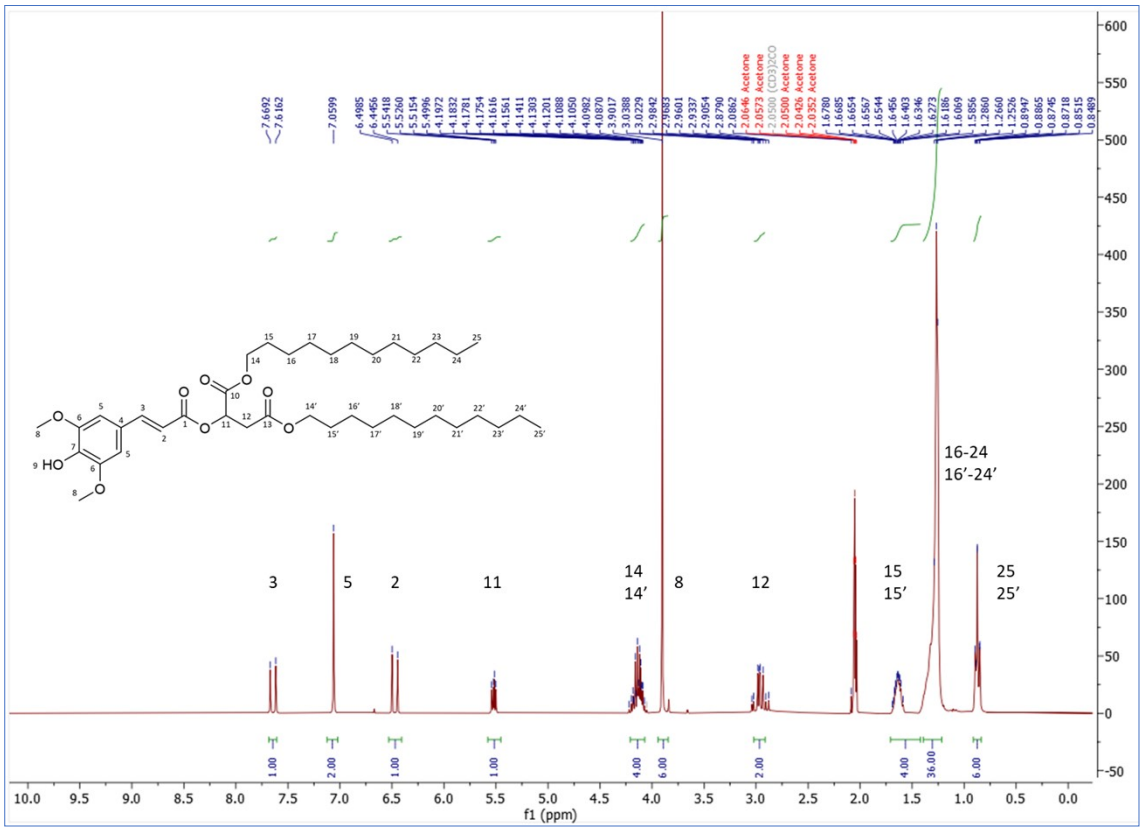

Figure S7: ^{1}H spectrum of dilauryl sinapoyl-L-malate.

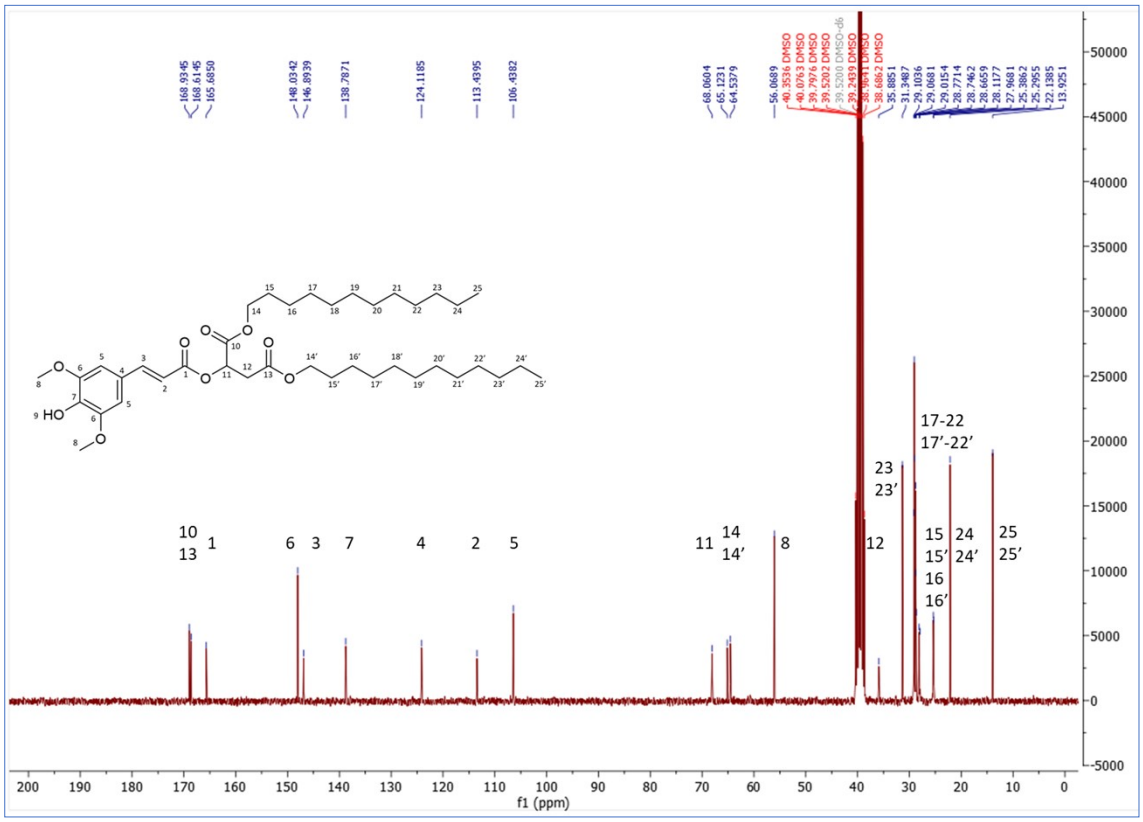

Figure S8: ^{13}C spectrum of dilauryl sinapoyl-L-malate.

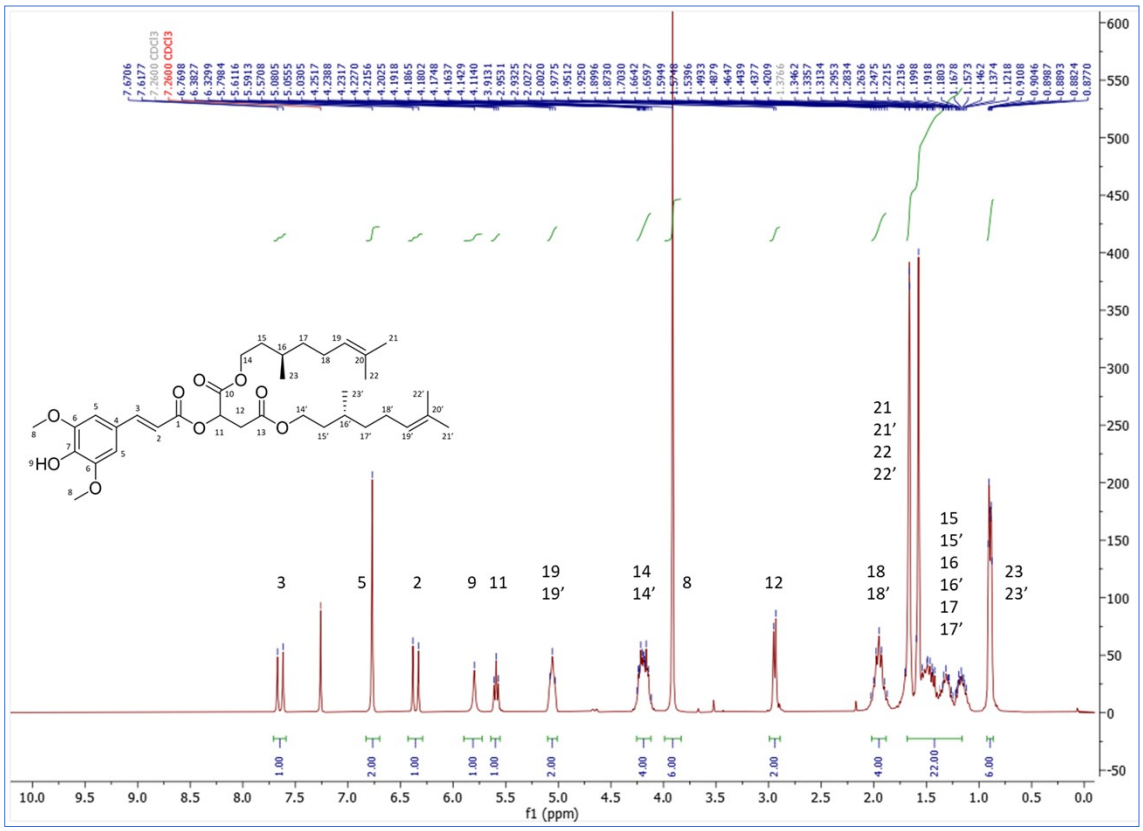

Figure S9: ^{1}H spectrum of dicitronellyl sinapoyl-L-malate.

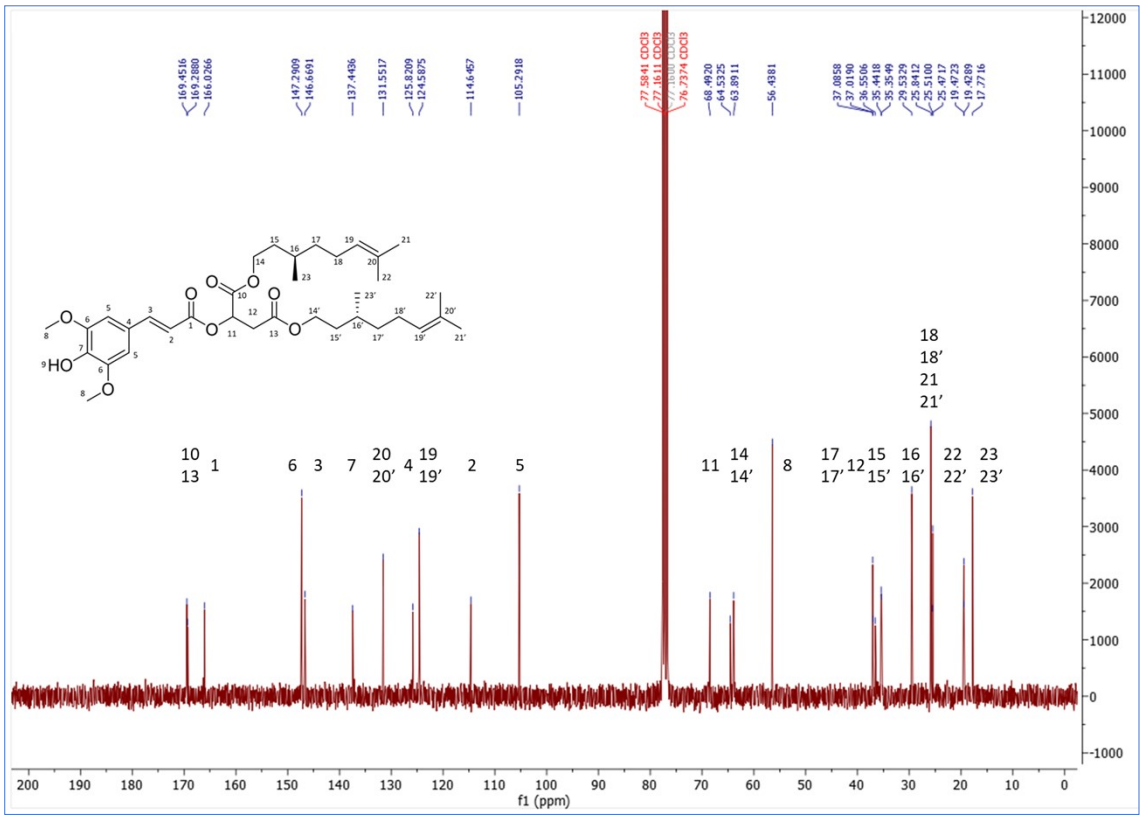

Figure S10: ^{13}C spectrum of dicitronellyl sinapoyl-L-malate.

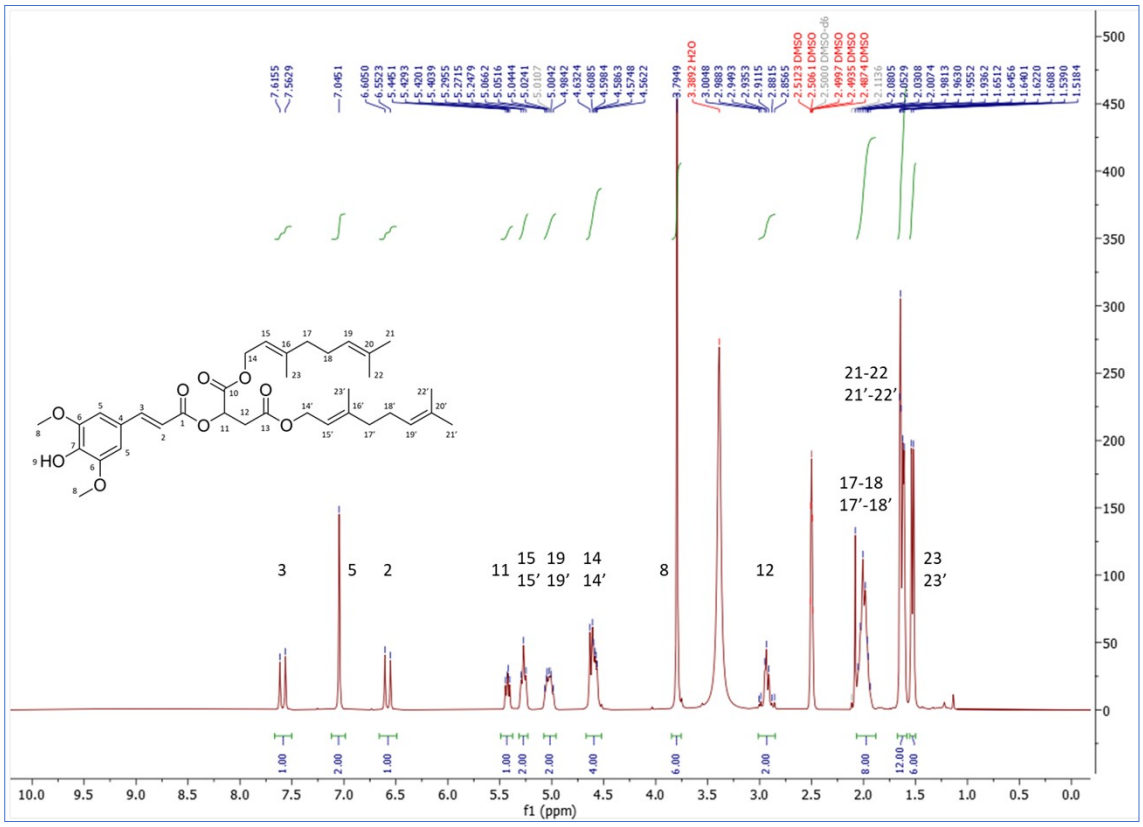

Figure S 11: ^{1}H spectrum of digeranyl sinapoyl-L-malate.

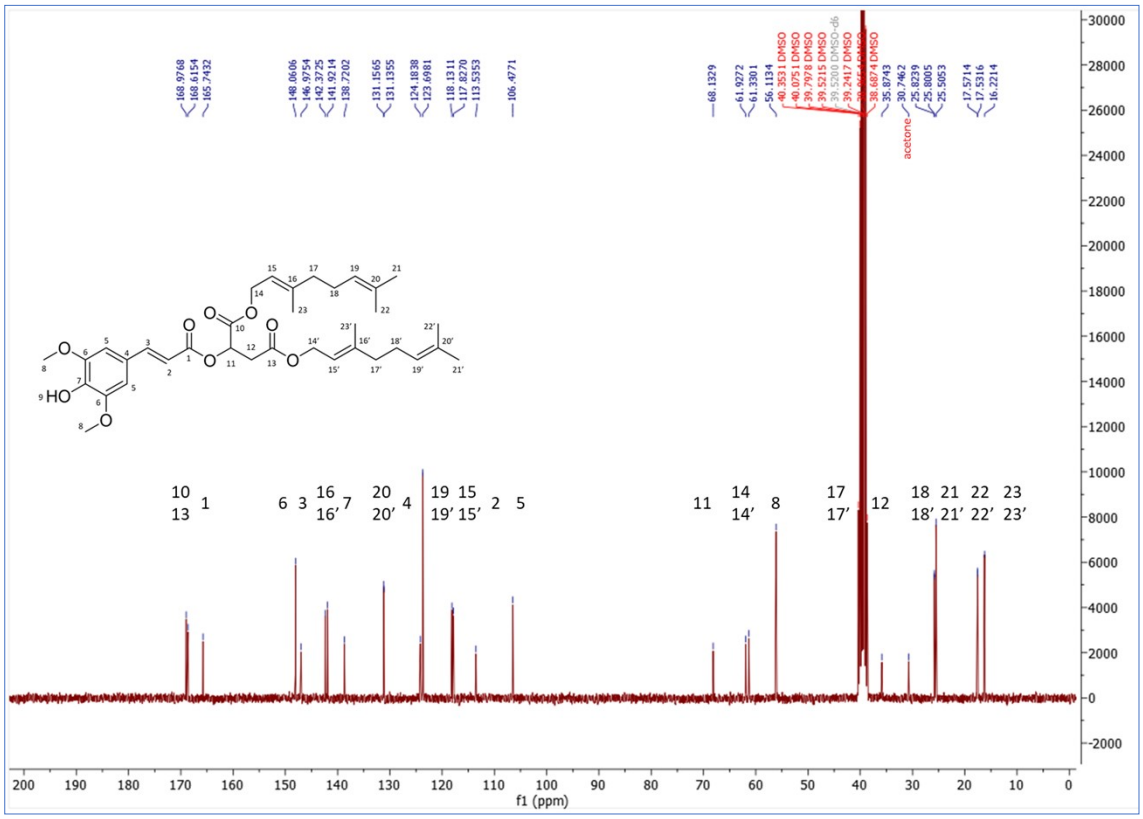

Figure S12: ^{13}C spectrum of digeranyl sinapoyl-L-malate.

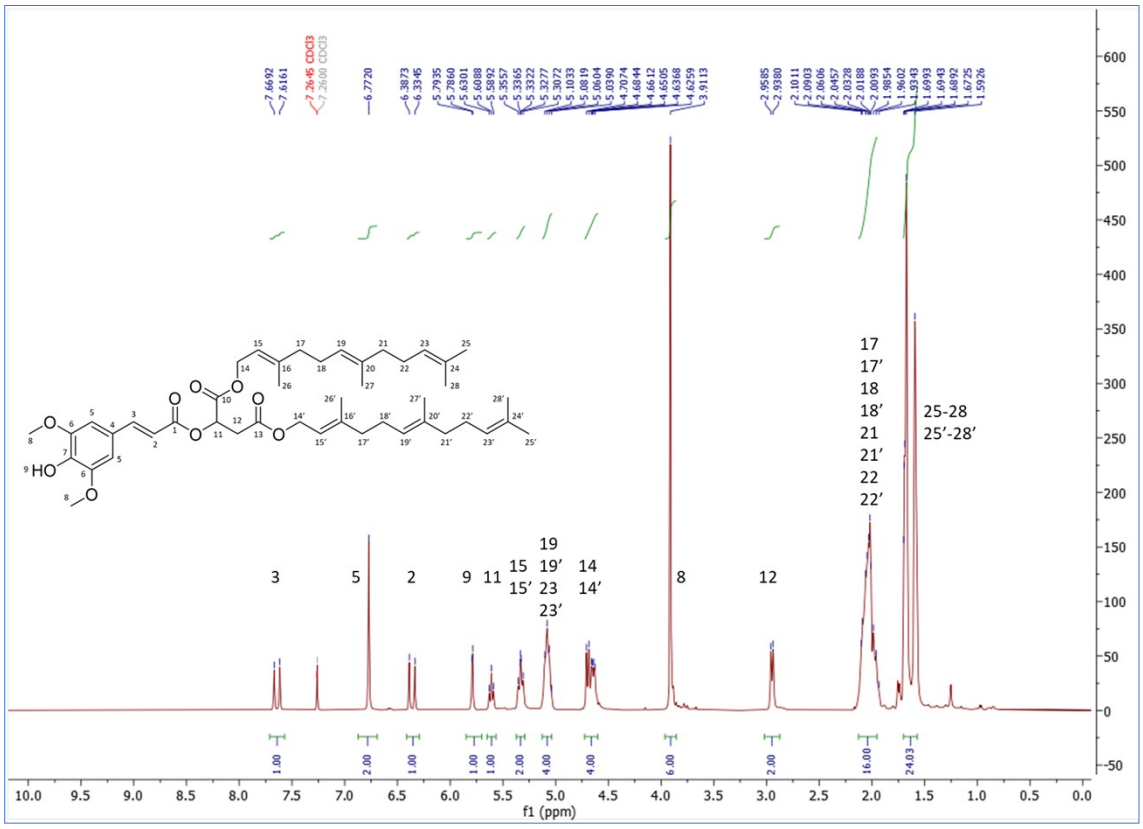

Figure S13: ^{1}H spectrum of difarnesyl sinapoyl-L-malate.

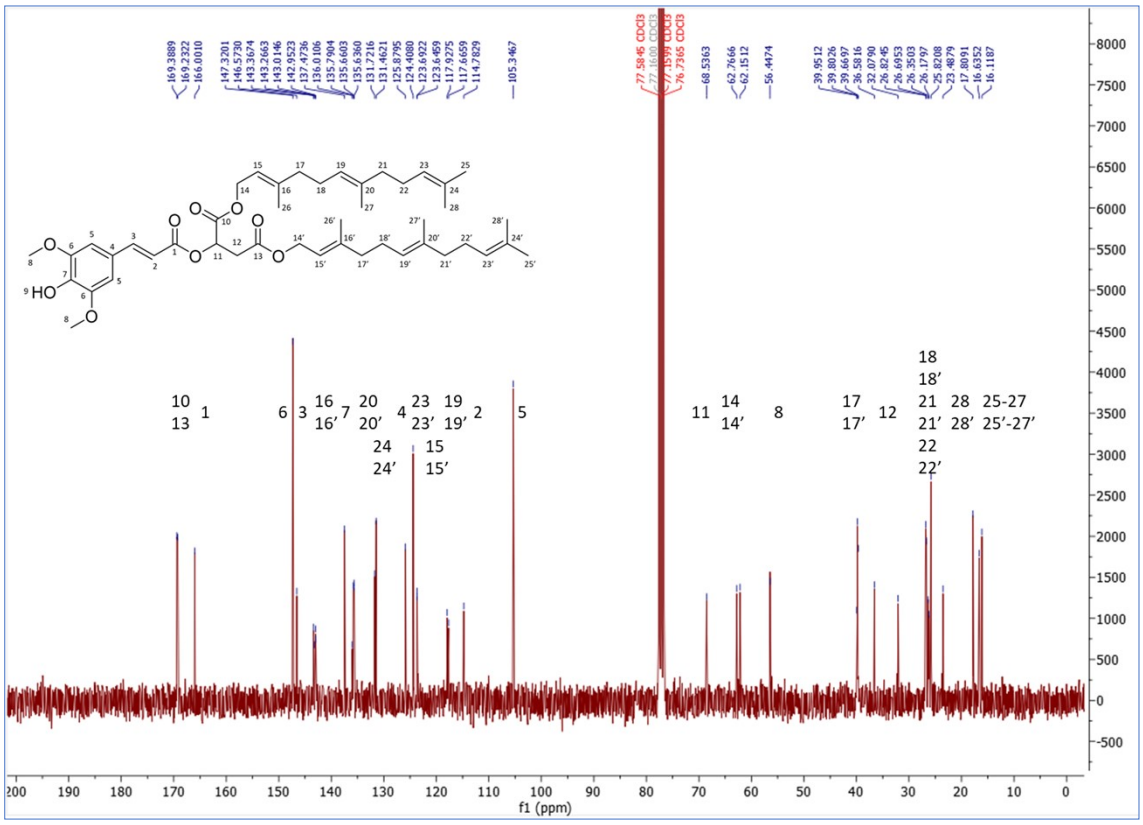

Figure S14: ^{13}C spectrum of difarnesyl sinapoyl-L-malate.

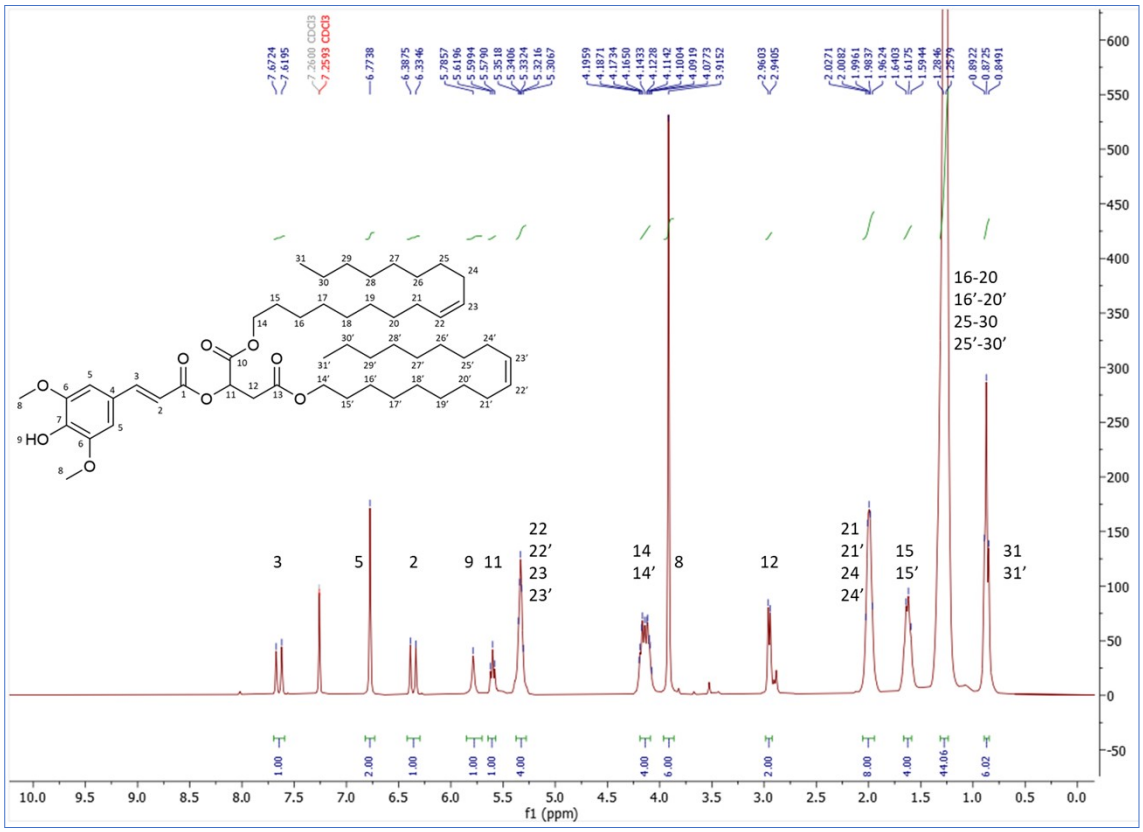

Figure S 15: ^{1}H spectrum of dioleylyl sinapoyl-L-malate.

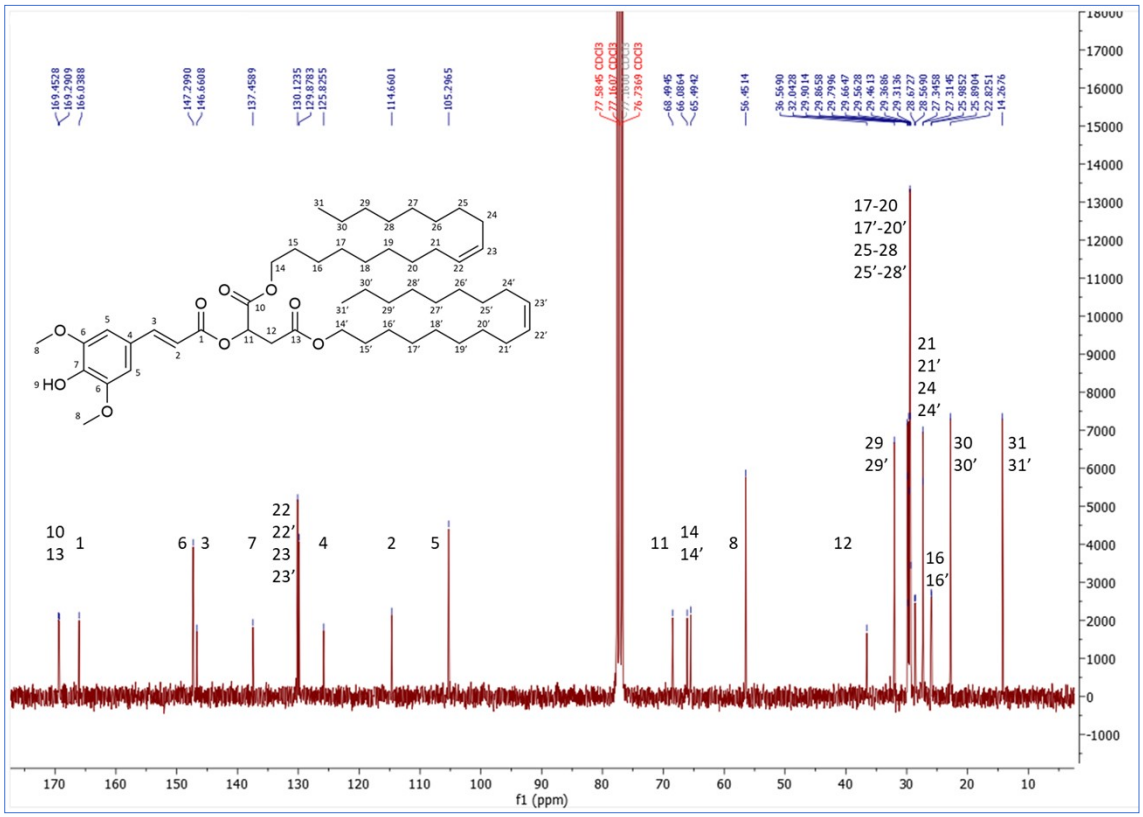

Figure S16: ^{13}C spectrum of dioleylyl sinapoyl-L-malate.

HRMS spectra of diester sinapoyl-L-malate

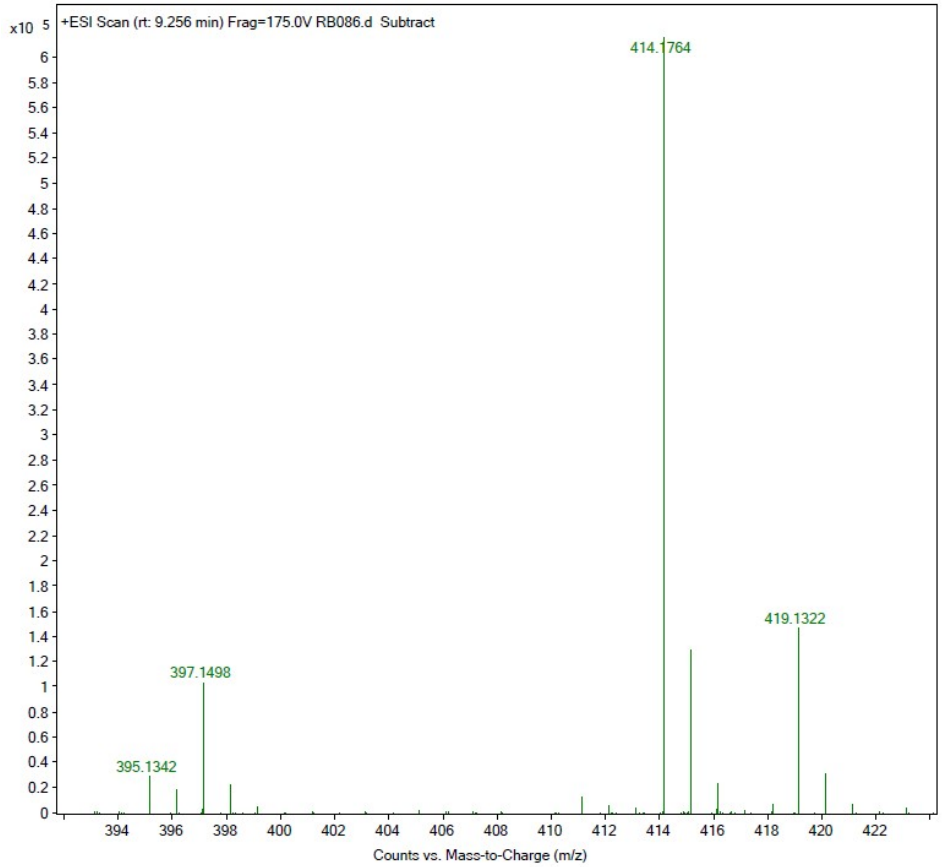

Figure S17: HRMS spectrum of diethyl sinapoyl-L-malate.

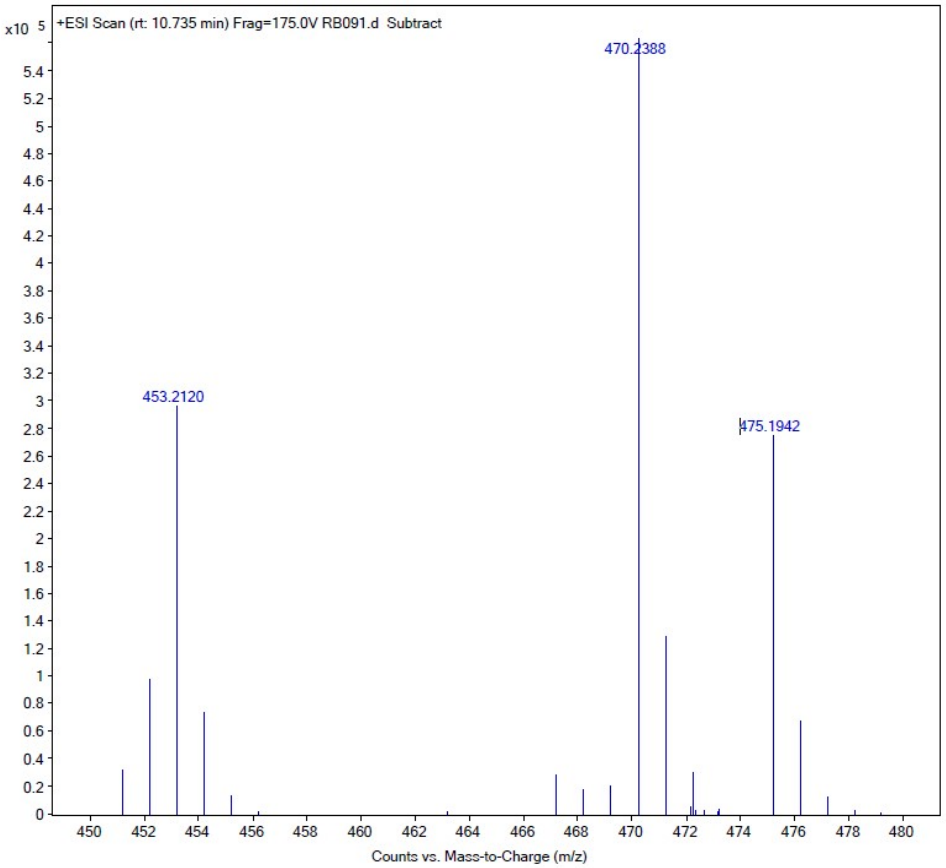

Figure S18: HRMS spectrum of dibutyl sinapoyl-L-malate.

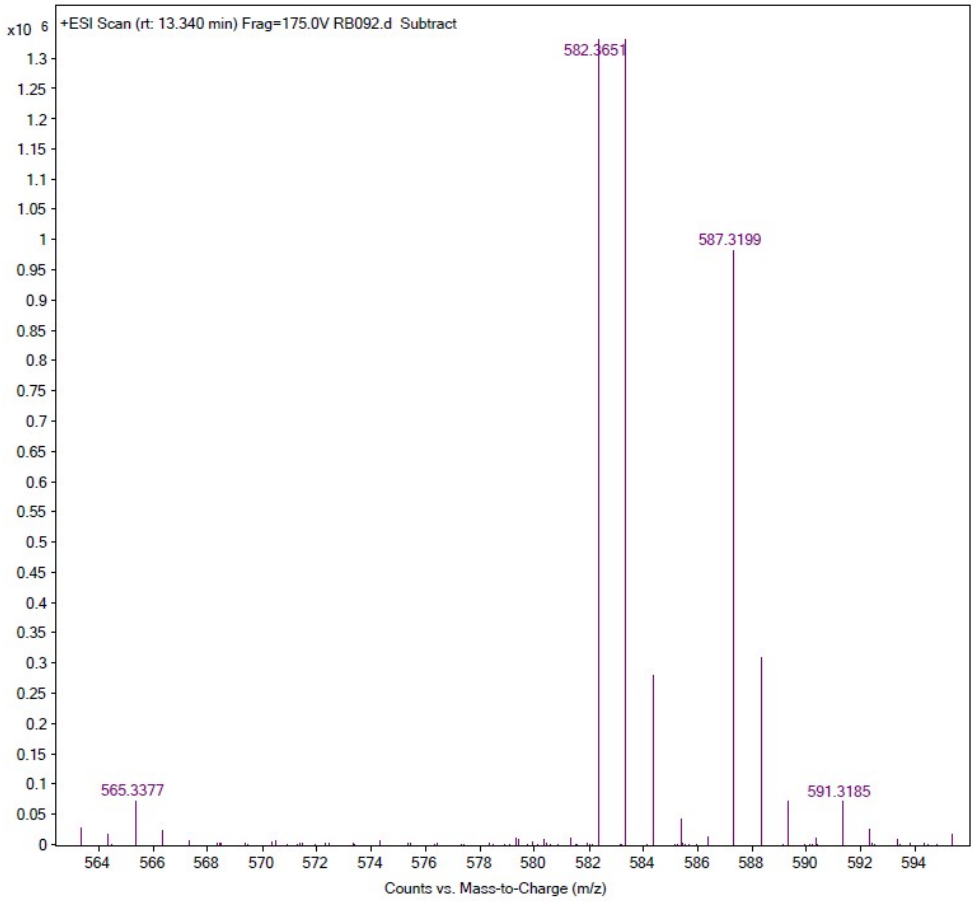

Figure S19: HRMS spectrum of dioctyl sinapoyl-L-malate.

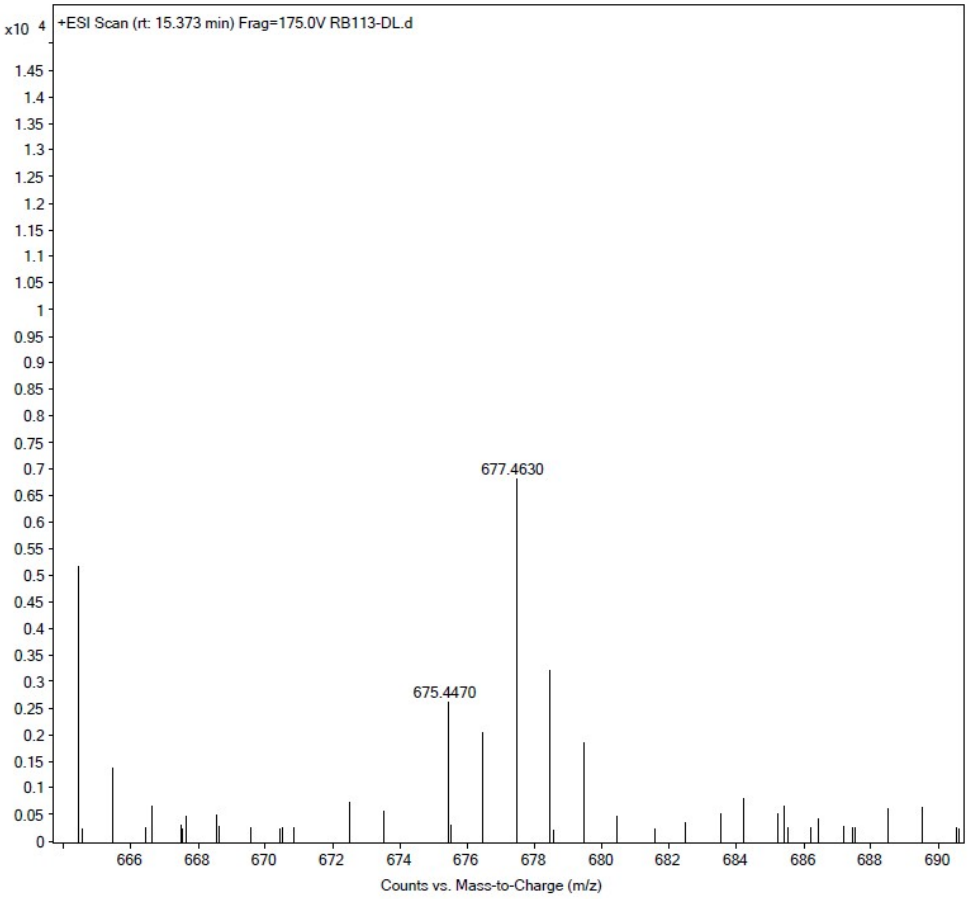

Figure S20: HRMS spectrum of dilauryl sinapoyl-L-malate.

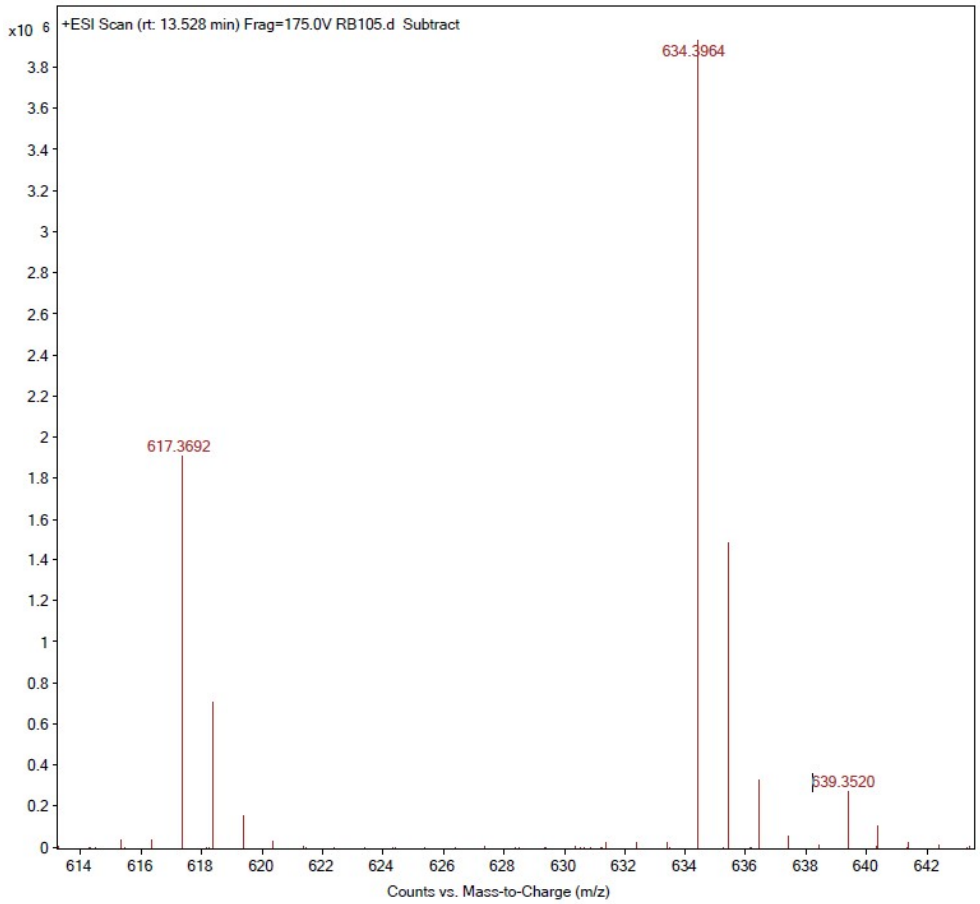

Figure S21: HRMS spectrum of dicitronellyl sinapoyl-L-malate.

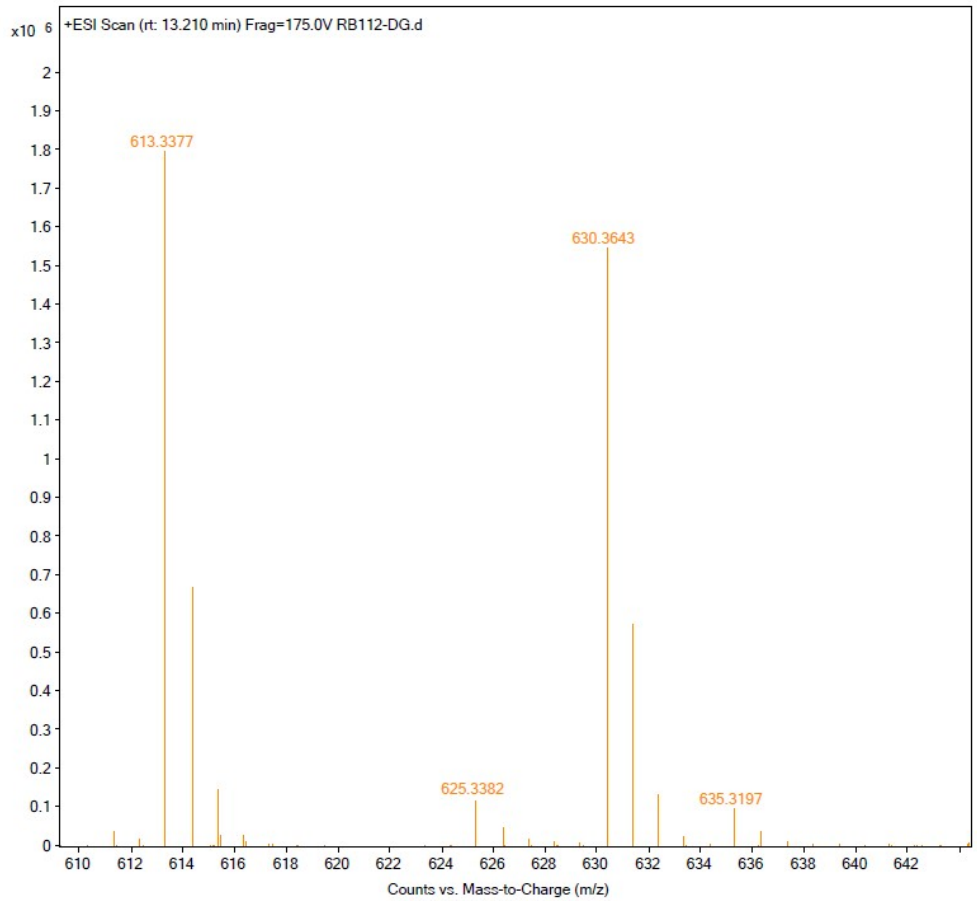

Figure S22: HRMS spectrum of digeranyl sinapoyl-L-malate.

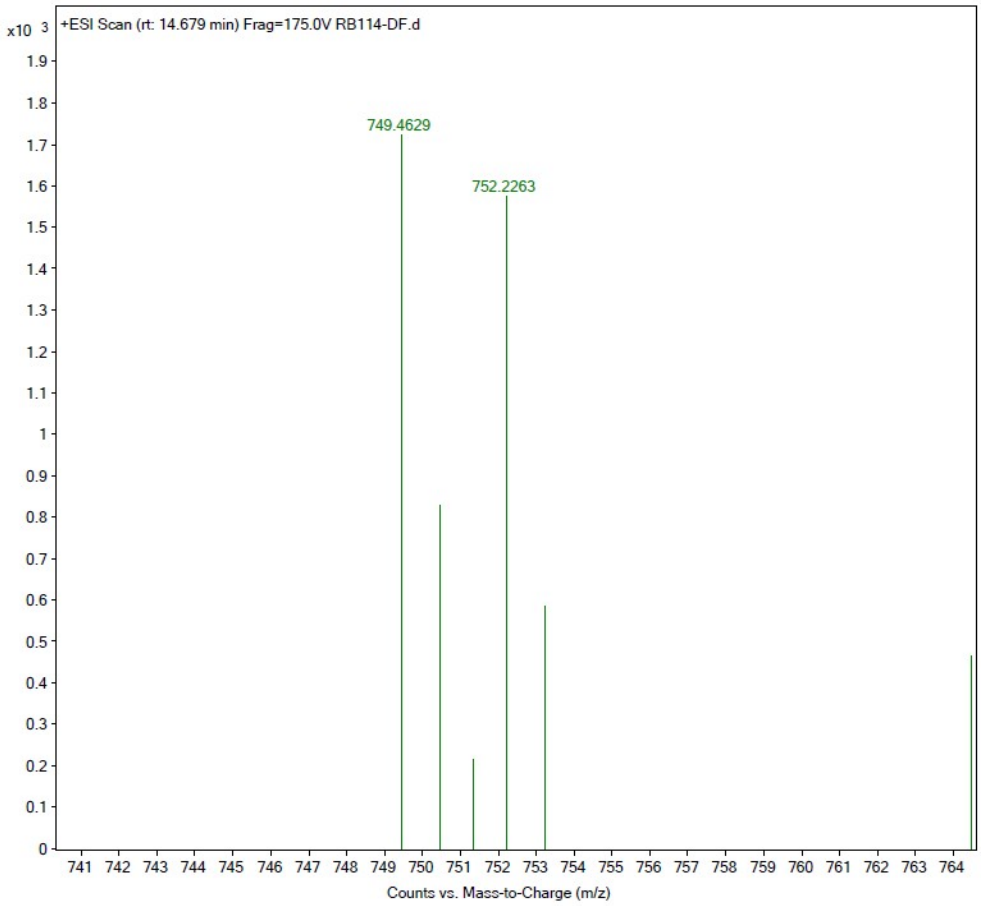

Figure S23: HRMS spectrum of difarnesyl sinapoyl-L-malate.

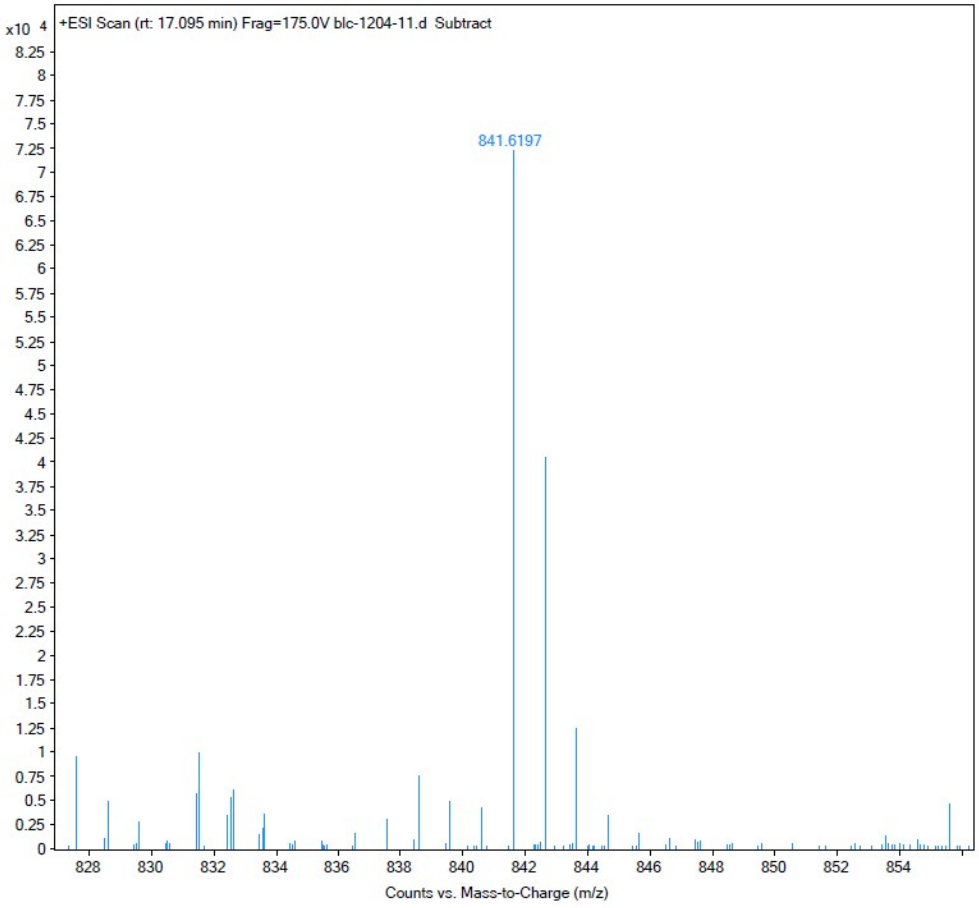

Figure S24: HRMS spectrum of dioleylyl sinapoyl-L-malate.

UV-Photostability spectra of diester sinapoyl-L-malate

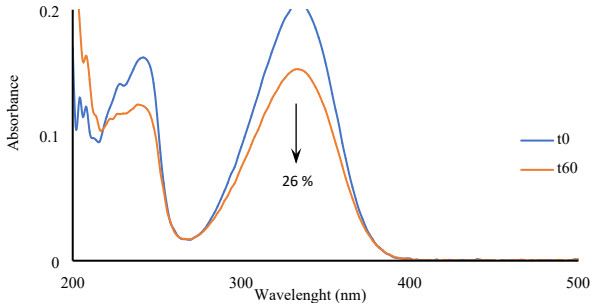

Figure S25: UV Photostability of diethyl sinapoyl-L-malate.

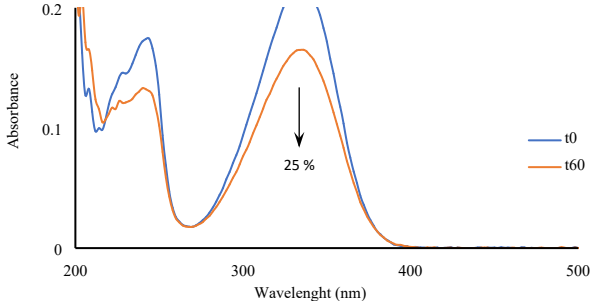

Figure S26: UV Photostability of dibutyl sinapoyl-L-malate.

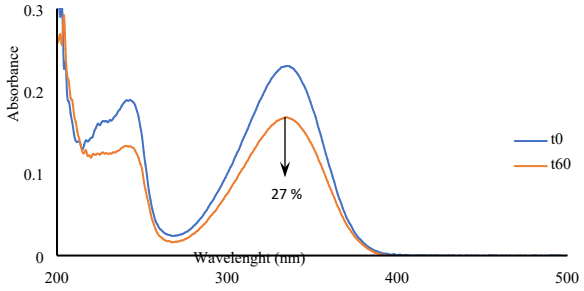

Figure S27: UV Photostability of dioctyl sinapoyl-L-malate.

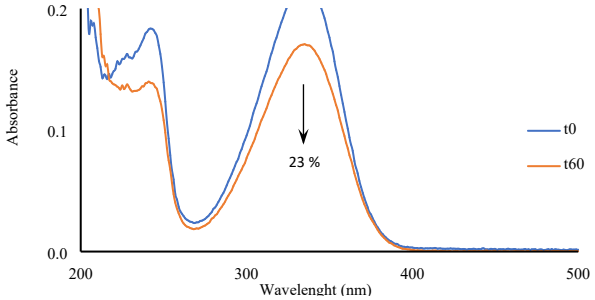

Figure S28: UV Photostability of dilauryl sinapoyl-L-malate.

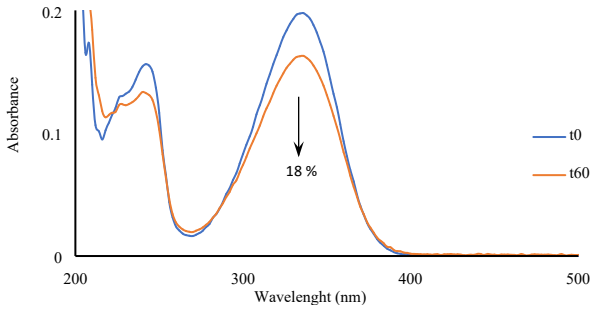

Figure S29: UV Photostability of dicitronellyl sinapoyl-L-malate.

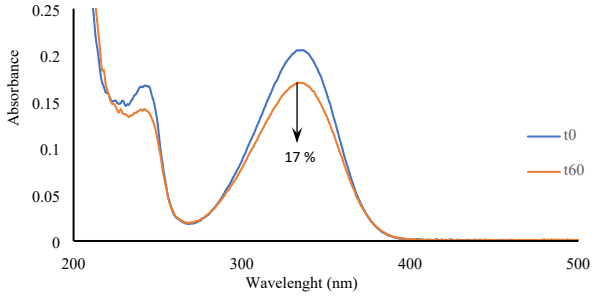

Figure S30: UV Photostability of digeranyl sinapoyl-L-malate.

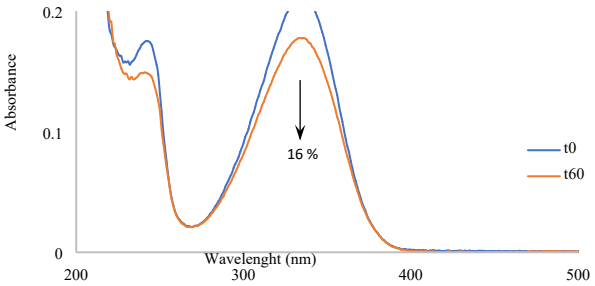

Figure S31: UV Photostability of difarnesyl sinapoyl-L-malate.

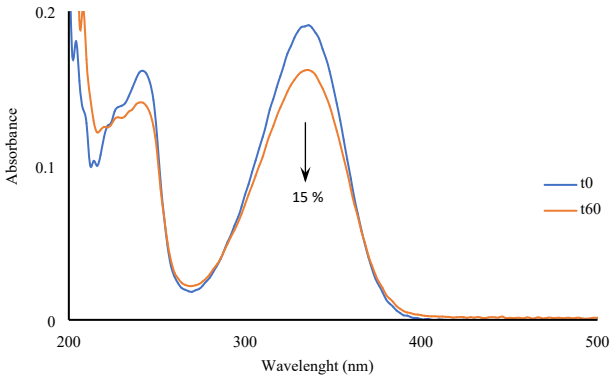

Figure S32: UV Photostability of dioleylyl sinapoyl-L-malate.

Antiradical activities

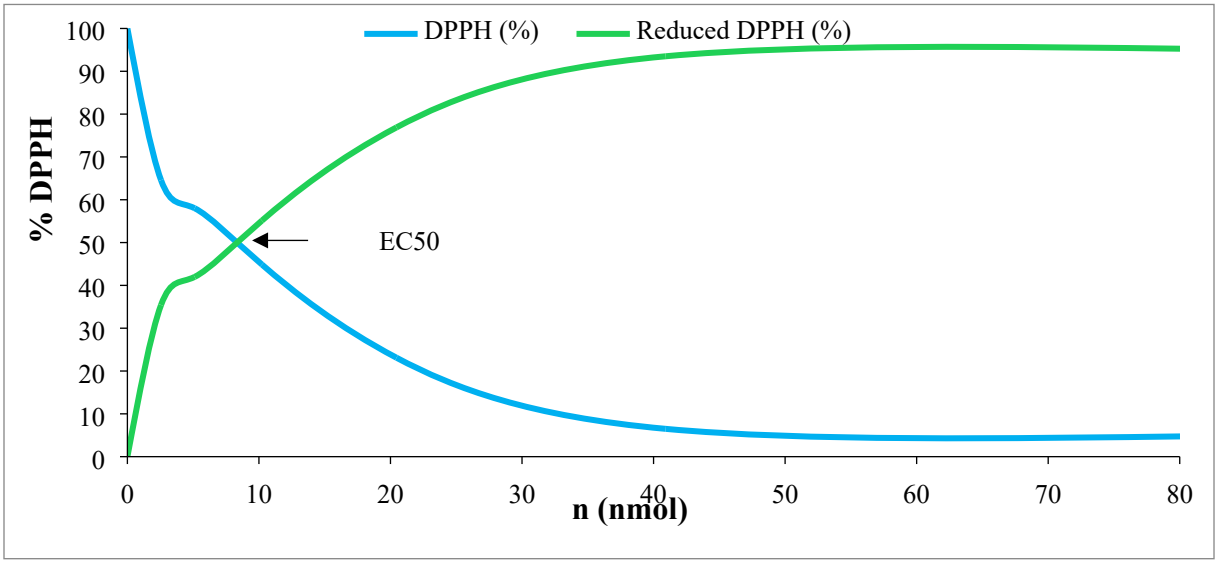

Figure S33: Antiradical activity of sinapoyl-L-malate

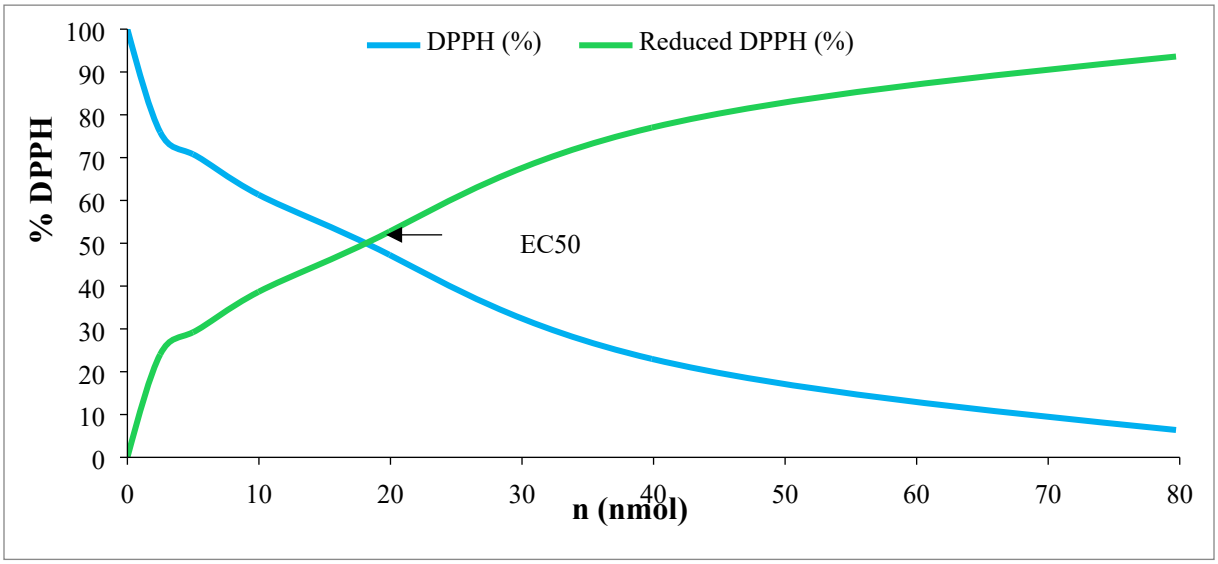

Figure S34: Antiradical activity of diethyl sinapoyl-L-malate.

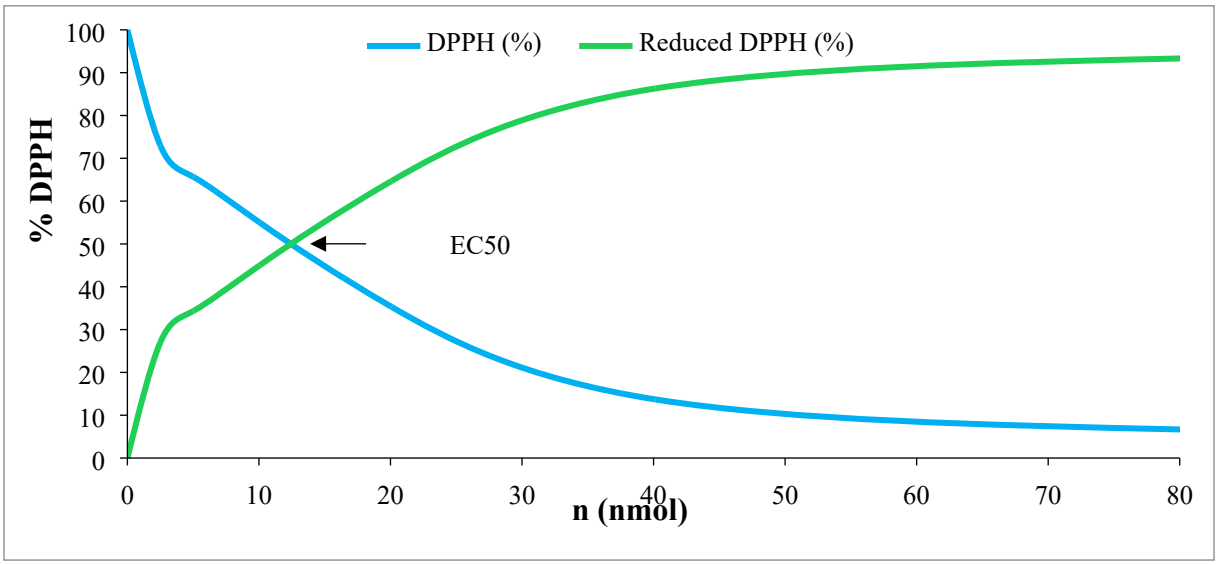

Figure S35: Antiradical activity of dibutyl sinapoyl-L-malate.

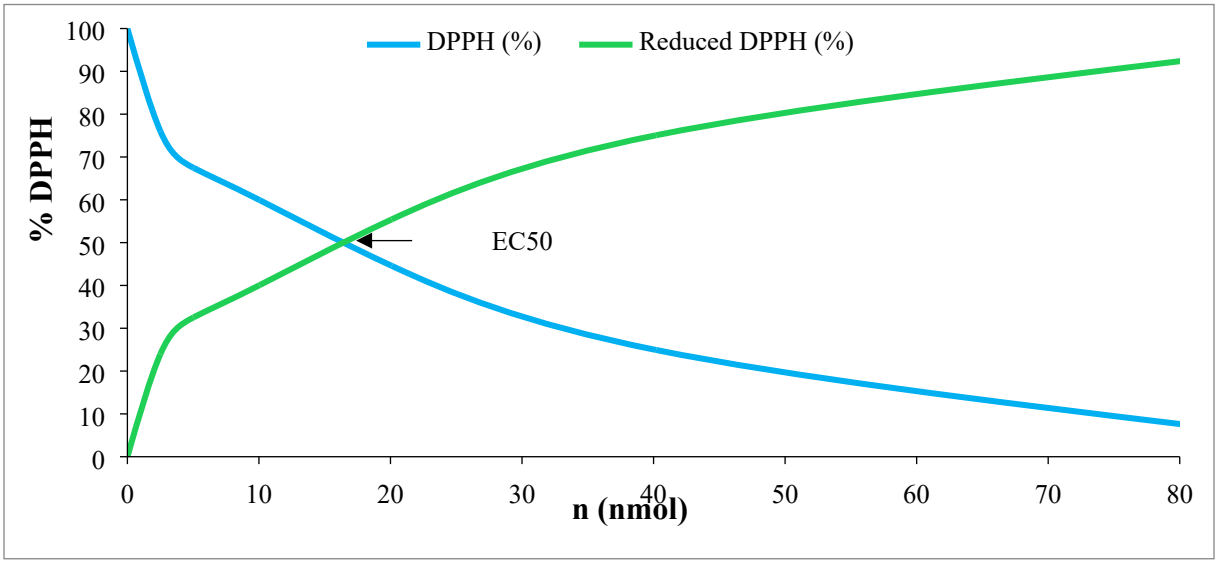

Figure S36: Antiradical activity dioctyl sinapoyl-L-malate.

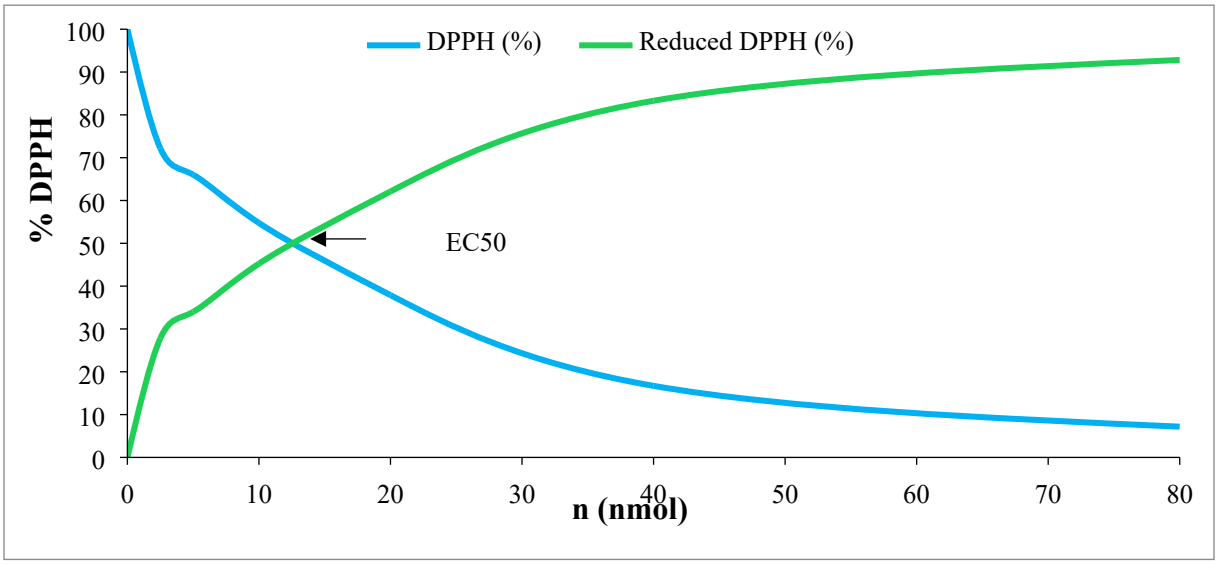

Figure S37: Antiradical activity of dilauryl sinapoyl-L-malate.

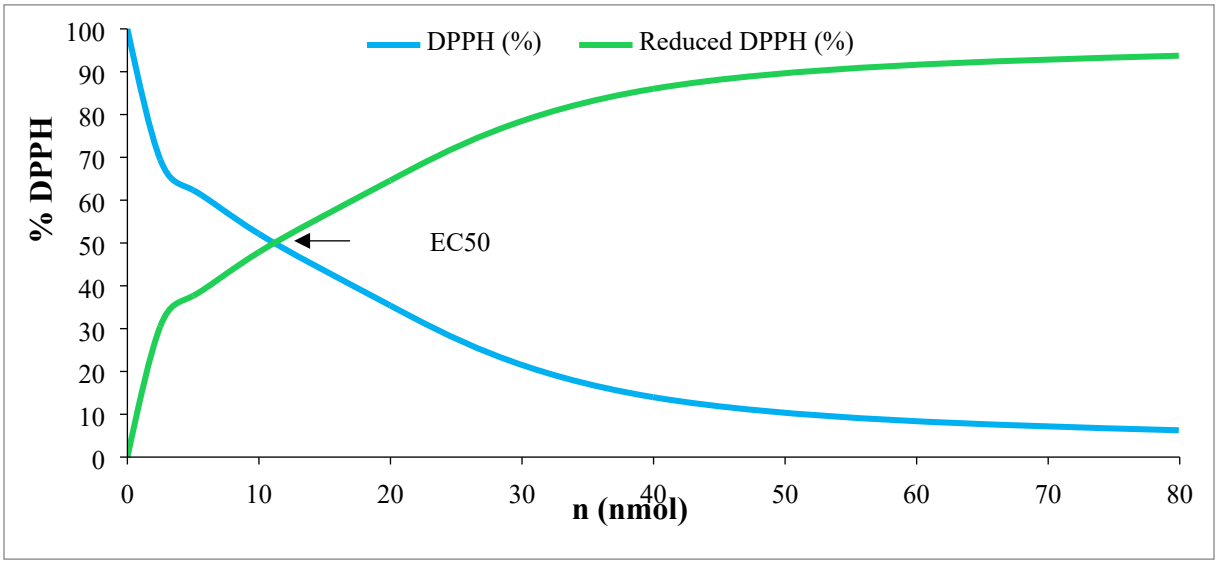

Figure S38: Antiradical activity of dicitronellyl sinapoyl-L-malate.

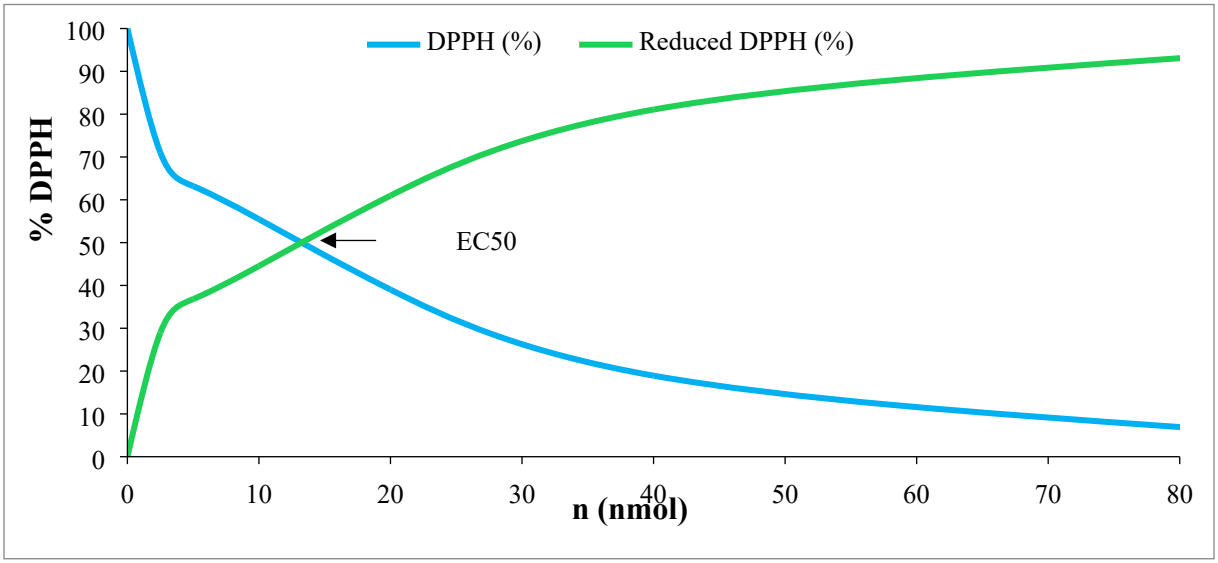

Figure S39: Antiradical activity of digeranyl sinapoyl-L-malate.

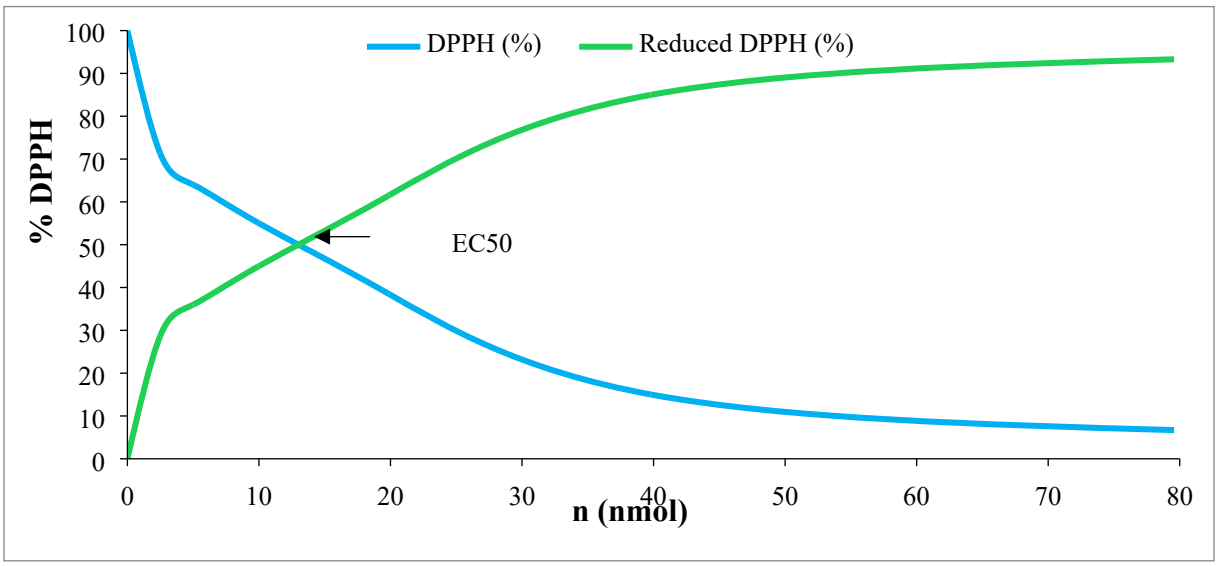

Figure S40: Antiradical activity of difarnesyl sinapoyl-L-malate.

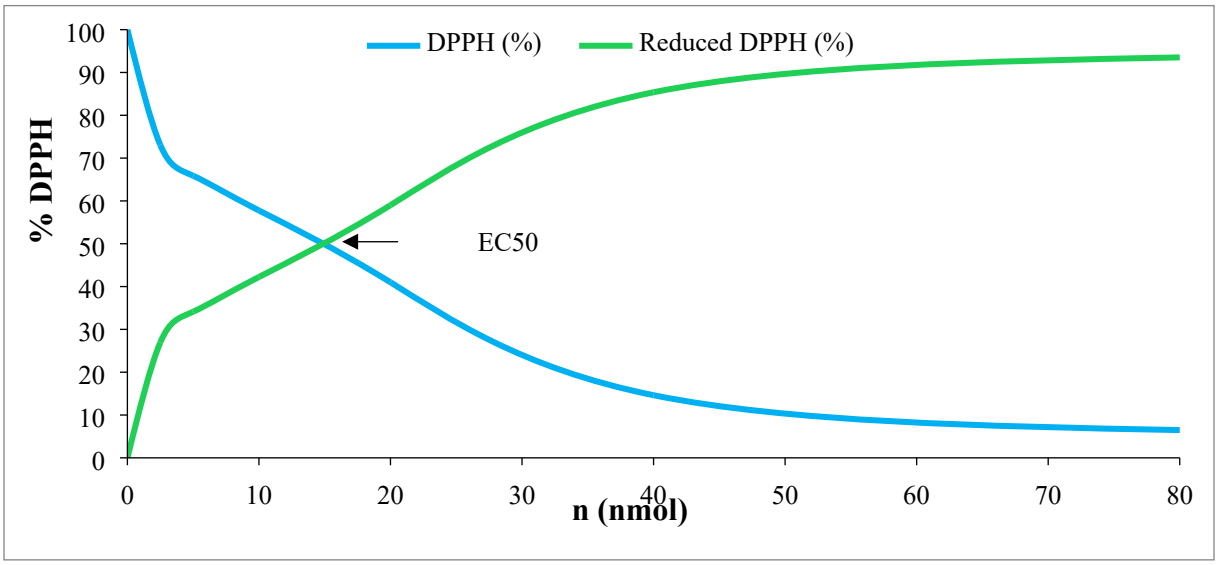

Figure S41: Antiradical activity of dioleylyl sinapoyl-L-malate.

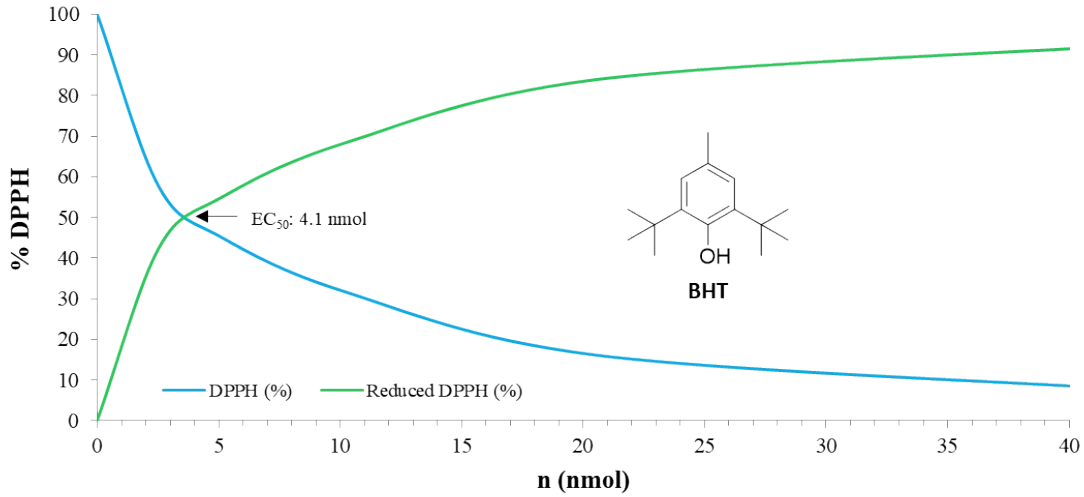

Figure S42: Antiradical activity of butylated hydroxytoluene.

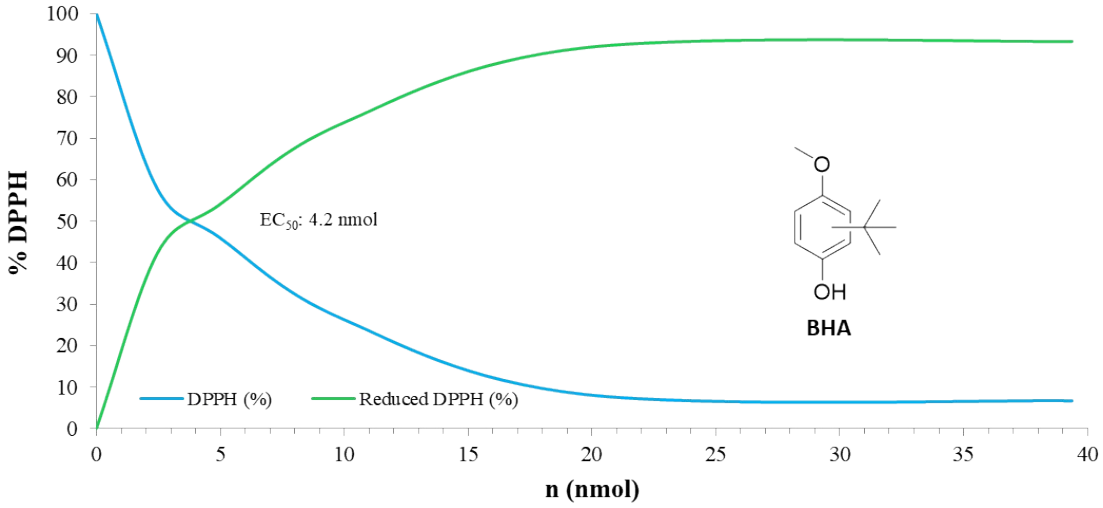

Figure S43: Antiradical activity of butylated hydroxyanisole.

Simulated Solar irradiation experiments

An ABET Technologies Sun 2000 solar simulator is used for irradiation experiments and provides a 0.96 solar equivalent power spectrum. Figure S44 shows that this lamp has a broad spectrum well correlated to the actual solar spectrum observed at sea level.

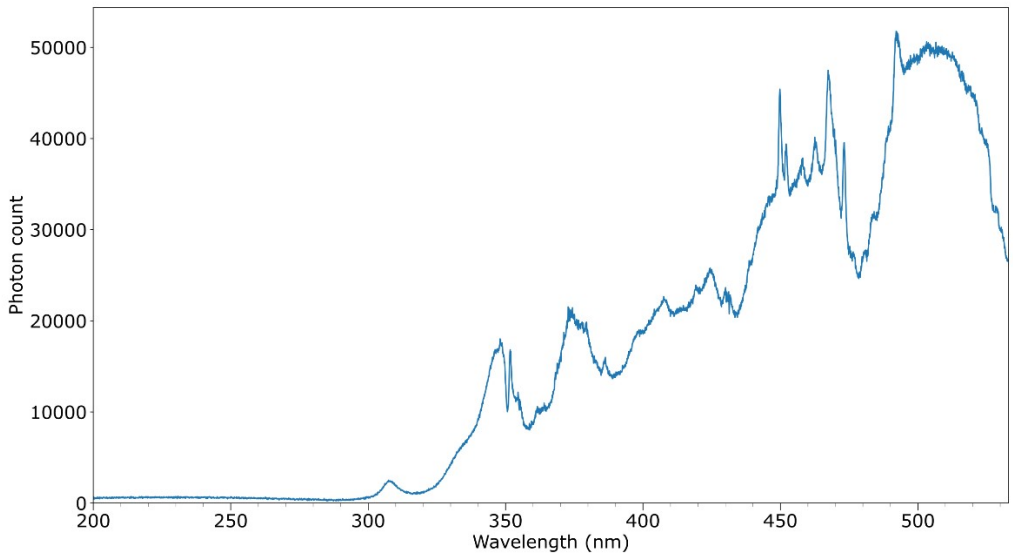

Figure S44: Measured ABET Technologies Sun 2000 solar simulator lamp spectrum.

Infrared Ion Spectroscopy vibrational analysis of DOSM

In this supplementary information, we discuss the computed vibrational bands of figure 5 in the main publication.

We begin by analyzing the spectrum of the protonated ion. The absence of a strong carbonyl stretching band near 1800 cm^{-1} suggests that the protonation of DO2HS involves a proton-shared motif that includes both carboxylic acid groups. The spectral match between computed and experimental spectra confirms that the two carboxylics are hydrogen bonded, as seen in Figure S45. Examining other significant features in the spectrum, we observe an intense doublet near 1350 cm^{-1}, attributed to the two CH_2 wagging vibrations of both octyl chains. The doublet at 1450 cm^{-1} is due to the CH_2 scissoring vibrations on both octyl chains directly attached to the ester function. This is in combination with an OH stretch vibration of the proton captured between the carboxylic functions. Its shoulder feature at 1550 cm^{-1} is attributed to an OH bending mode of the captured proton, for which a second mode is observed at 1200 cm^{-1}. This last feature is also attributable to a CH_2 waging mode of the octyl groups. Lastly, the feature at 1150 cm^{-1} is attributed to a C-O stretching vibration of the hydroxyl group on DO2HS.

For Na^+-DO2HS, an intense vibration at 1725 cm^{-1} is observed, which can be attributed to the C=O stretching vibrations of either ester group in DO2HS. Within the triplet feature centered at 1400 cm^{-1}, the peak closest to 1500 cm^{-1} corresponds to the CH_2 scissoring of the methylene group attached to the ester function of the octyl 3-hydroxypropanoate ester moiety. The other two peaks in the triplet are associated with different CH_2 wagging modes of the same ester moiety. There is a broad and prominent peak at 1230 cm^{-1}, comprising three absorption bands. The most intense absorption at 1300 cm^{-1} is due to an OH bending mode combined with CH_2 wagging of the methylene between the ester functions. The two remaining absorption bands are due to a CH bending mode of the same moieties.

Additionally, two more vibrational modes result in a shoulder feature slightly above 1300 cm^{-1}. The first mode comprises a combination of CH bending and CH_2 twisting of both octyl chains, while the second mode is a delocalized CH bending mode of the entire molecule. We can observe two peaks below 1100 cm^{-1}. The peak at 950 cm^{-1} is attributed to the CH_2 wagging of the octyl 3-hydroxy-propanoate ester moiety, while the one at 1100 cm^{-1} is caused by CH_2 twisting in the methylene functionality in between the two ester functions.

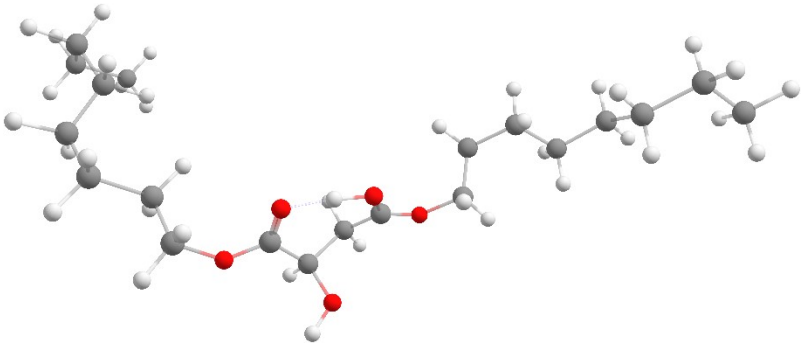

Figure S45: 3D computed structure of DG2HS depicting hydrogen bonding between the two carboxyl groups.

Infrared Ion Spectroscopy vibrational analysis of DGSM

In this supplementary information, we discuss the computed vibrational bands of figure 6 in the main publication.

The geraniol esters exhibit two C=C stretch vibrations, causing the feature at 1650 cm^{-1}, while the C=O stretch of the 3-hydroxybutyrate moiety carries the carboxylic stretch at 1725 cm^{-1}. The second carboxylic vibration, involving both carbonyls coordinating with the cesium atom, produces the shoulder at lower wavenumbers.

The right-side peak of the doublet at 1415 cm^{-1} results from a combination of CH bending and wagging vibrations of the two geraniol tails. The peak on the left side is attributed to the CH_2 wagging vibration of the two CH_2 moieties of the 3-hydroxybutyrate moiety combined with an O-H bending vibration, resulting in only one absorption band responsible for the feature.

The measured spectrum displays a strong band at 1205 cm^{-1}, comprising two unresolved features and another feature at 1275 cm^{-1}. This was observed when measured with a wavelength step of 3 cm^{-1} and reduced laser power. Upon examining the computed spectrum of DG2HS, a similar peak pattern was found, with a slightly higher predicted wavenumber for the absorption band in the center. The first peak is due to the O-H bending vibration, while the second peak is attributed to a secondary OH bending mode combined with the CH_2 wagging of the CH_2 group sandwiched between the esters. The third peak of the triplet is due to the twisting vibration of both CH_2 groups of the geraniol tails, which are directly attached to the ester moieties.

At lower wavenumbers, two distinct peaks in the IRIS spectrum provide significant information about the sample. The first peak is observed at 1090 cm^{-1} and is attributed to the C-O stretching of the alcohol. A minor shoulder is also observed at 1040 cm^{-1}, caused by a CH_2 twisting vibration of the CH_2 group between the esters. The second peak is observed at 919 cm^{-1} and is attributed to two CH bending vibrations of the double bond CH groups closest to the central esters of the two geraniol tails. Although the experiment-versus-theory match for this band is not perfect, we conclude that DG2HS is the primary degradation product of DGSM based on the information provided by the IRIS spectrum.

Toxicology

Table S1. Translation of the VEGA, TEST and LAZAR predictions into a mutagenicity/carcinogenicity score.

Prediction	Reliability	Score
mutagenic/carcinogenic	experimental data	1
mutagenic/carcinogenic	good reliability	0.9
possible mutagenic/carcinogenic	good reliability	0.8
mutagenic/carcinogenic	moderate reliability	0.7
possible mutagenic/carcinogenic	moderate reliability	0.6
(possible) mutagenic/carcinogenic	low reliability	0.5
(possible) non-mutagenic/non-carcinogenic	low reliability	0.5
possible non-mutagenic/non-carcinogenic	moderate reliability	0.4
non-mutagenic/non-carcinogenic	moderate reliability	0.3
possible non-mutagenic/non-carcinogenic	good reliability	0.2
non-mutagenic/non-carcinogenic	good reliability	0.1
non-mutagenic/non-carcinogenic	experimental data	0

Table S2. Translation of the VEGA predictions into a persistence score.

VEGA prediction	Reliability	Score
persistent	experimental data	1
P/vP or vP or >120 days or >40 days	good reliability	0.9
P/vP or vP or >120 days or >40 days	moderate reliability	0.7
P/vP or vP or >120 days or >40 days	low reliability	0.5
nP or nP/P or <120 days or <40 days	low reliability	0.5
nP or nP/P or <120 days or <40 days	moderate reliability	0.3
nP or nP/P or <120 days or <40 days	good reliability	0.1
non-persistent	experimental data	0

Table S3. Translation of the ISIDA predictions into a persistence score.

ISIDA prediction	Reliability	Score
persistent	experimental data	1
persistent	optimal reliability	0.9
persistent	good reliability	0.766
persistent	average reliability	0.633
persistent	outside AD	0.5
non-persistent	outside AD	0.5
non-persistent	average reliability	0.366
non-persistent	good reliability	0.233
non-persistent	optimal reliability	0.1
non-persistent	experimental data	0

Table S4. Predictions on the endocrine toxicity using VEGA platform.

Substance	VEGA computational model	Prediction	Reliability
SM	Estrogen Receptor Relative Binding Affinity	active	low
	Estrogen Receptor-mediated effect	inactive	good
	Androgen Receptor-mediated effect	inactive	moderate
	Thyroid Receptor Alpha effect	inactive	good
	Thyroid Receptor Beta effect	inactive	good
DESM	Estrogen Receptor Relative Binding Affinity	active	low
	Estrogen Receptor-mediated effect	inactive	good

	Androgen Receptor-mediated effect	inactive	moderate
	Thyroid Receptor Alpha effect	inactive	good
	Thyroid Receptor Beta effect	inactive	good
DBSM	Estrogen Receptor Relative Binding Affinity	active	low
	Estrogen Receptor-mediated effect	inactive	good
	Androgen Receptor-mediated effect	inactive	moderate
	Thyroid Receptor Alpha effect	inactive	good
	Thyroid Receptor Beta effect	inactive	good
DOSM	Estrogen Receptor Relative Binding Affinity	active	low
	Estrogen Receptor-mediated effect	inactive	good
	Androgen Receptor-mediated effect	inactive	moderate
	Thyroid Receptor Alpha effect	inactive	good
	Thyroid Receptor Beta effect	inactive	good
DOleySM	Estrogen Receptor Relative Binding Affinity	active	low
	Estrogen Receptor-mediated effect	inactive	good
	Androgen Receptor-mediated effect	inactive	moderate
	Thyroid Receptor Alpha effect	inactive	good
	Thyroid Receptor Beta effect	inactive	good
DCSM	Estrogen Receptor Relative Binding Affinity	active	low
	Estrogen Receptor-mediated effect	inactive	good
	Androgen Receptor-mediated effect	inactive	moderate
	Thyroid Receptor Alpha effect	inactive	good
	Thyroid Receptor Beta effect	inactive	good
DLSM	Estrogen Receptor Relative Binding Affinity	active	low
	Estrogen Receptor-mediated effect	inactive	good
	Androgen Receptor-mediated effect	inactive	moderate
	Thyroid Receptor Alpha effect	inactive	good
	Thyroid Receptor Beta effect	inactive	good
DGSM	Estrogen Receptor Relative Binding Affinity	active	low
	Estrogen Receptor-mediated effect	inactive	moderate
	Androgen Receptor-mediated effect	inactive	moderate
	Thyroid Receptor Alpha effect	inactive	good
	Thyroid Receptor Beta effect	inactive	good
DFSM	Estrogen Receptor Relative Binding Affinity	active	low
	Estrogen Receptor-mediated effect	inactive	good
	Androgen Receptor-mediated effect	inactive	moderate
	Thyroid Receptor Alpha effect	inactive	good
	Thyroid Receptor Beta effect	inactive	good

Table S5. Predicted oral LD_{50} and NOAEL in rats.

Substance	LD_{50} (mg/kg bw)	NOAEL (mg/kg bw per day)
SM	3380	580
DESM	2904	199
DBSM	4841	245
DOSM	8953	372
DOleySM	NA	1050
DCSM	9213	331
DLSM	12538	563
DGSM	1575	314
DFSM	580	438
DO2HS	14567	359
SAL	1982	67

NA: not applicable

Table S6: Predictions on the bioaccumulation property using VEGA and ISIDA Predictor platforms.

Substance	Log BCF computational model	Prediction	Reliability
SM	CAESAR	0.22	low
	Meylan	0.50	low
	KNN/Read-across	0.84	moderate
	Arnot-Gobas	-0.02	low
	ISIDA	0.13	good
DESM	CAESAR	0.27	low
	Meylan	1.33	low
	KNN/Read-across	1.43	low
	Arnot-Gobas	0.02	low
	ISIDA	0.64	good
DBSM	CAESAR	0.13	low
	Meylan	1.25	low
	KNN/Read-across	1.35	low
	Arnot-Gobas	0.25	low
	ISIDA	1.03	good
DOSM	CAESAR	0.27	low
	Meylan	2.84	low
	KNN/Read-across	0.96	low
	Arnot-Gobas	0.04	low
	ISIDA	1.06	good
DOleySM	CAESAR	-0.05	low
	Meylan	0.50	low
	KNN/Read-across	2.25	low
	Arnot-Gobas	-0.05	low
	ISIDA	1.53	good
DCSM	CAESAR	0.10	low
	Meylan	2.46	low
	KNN/Read-across	0.98	low
	Arnot-Gobas	-0.02	low
	ISIDA	1.17	good
DLSM	CAESAR	0.22	low
	Meylan	1.51	low
	KNN/Read-across	1.33	low
	Arnot-Gobas	-0.05	low
	ISIDA	1.15	good
DGSM	CAESAR	-0.18	low
	Meylan	3.10	low
	KNN/Read-across	1.76	low
	Arnot-Gobas	2.02	low
	ISIDA	1.30	good
DFSM	CAESAR	-0.02	low
	Meylan	0.53	low
	KNN/Read-across	1.47	low
	Arnot-Gobas	-0.05	low
	ISIDA	1.54	good

Table S7. Predictions on the biodegradability property using VEGA and ISIDA Predictor platforms.

Substance	VEGA	ISIDA
SM	RB (moderate)	nRB (low)
DESM	RB (moderate)	nRB (low)
DBSM	RB (moderate)	nRB (good)
DOSM	RB (moderate)	nRB (good)
DOleySM	RB (moderate)	nRB (good)
DCSM	RB (moderate)	nRB (good)
DLSM	RB (moderate)	nRB (good)
DGSM	RB (low)	nRB (average)
DFSM	RB (moderate)	nRB (good)

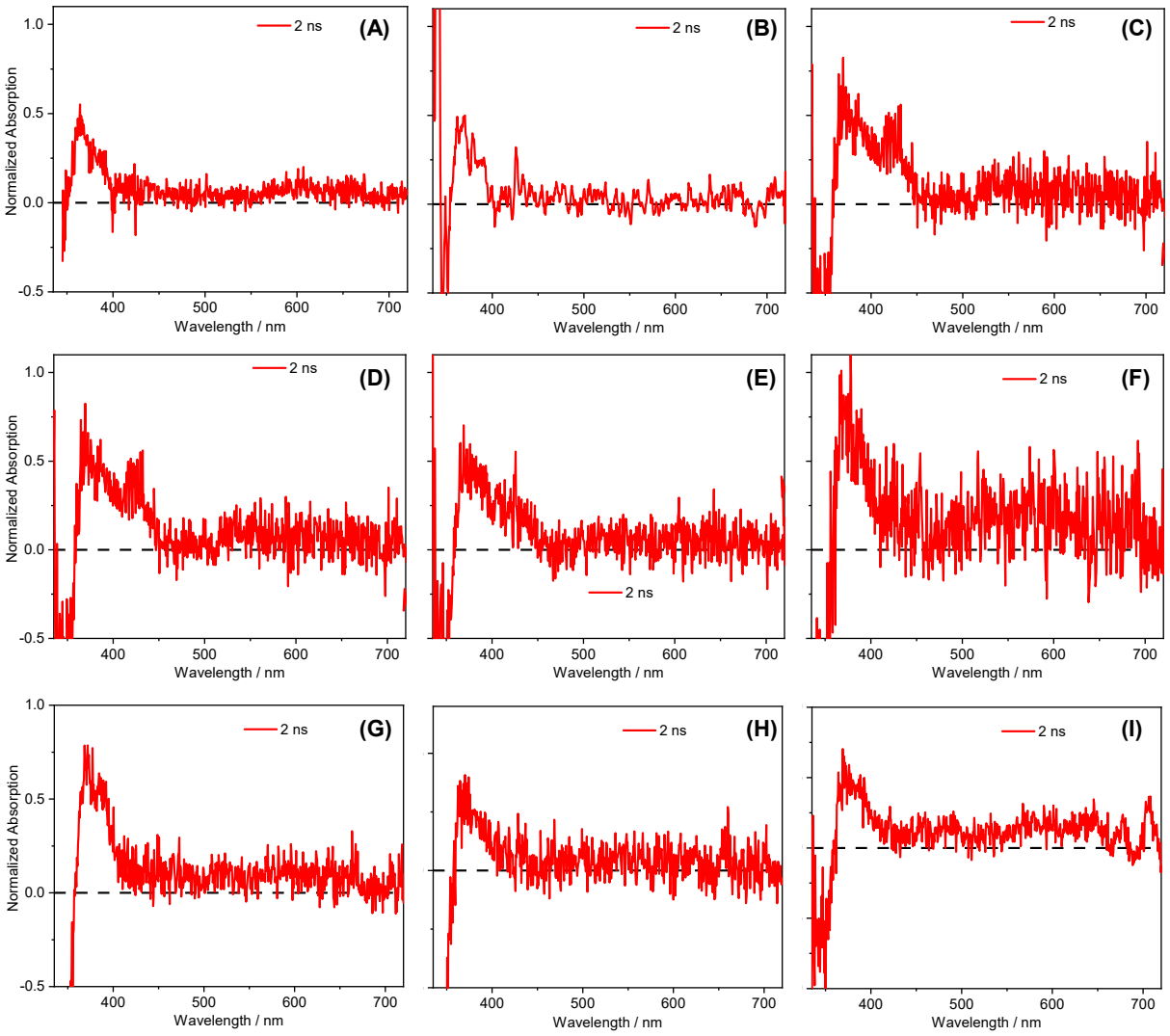

2 ns transient spectral of Sinapoyl-L-Malate and its derivatives

Figure S46: 2 ns transient data obtained in caprylic capric triglyceride for (A) SM, (B) DESM, (C) DBSM (D) DOSM, (E) DLSM, (F) DCSM, (G) DGSM, (H) DFSM, and (I) DOleySM

Evolution associated difference spectra (EADS) obtained from the global fitting of transient

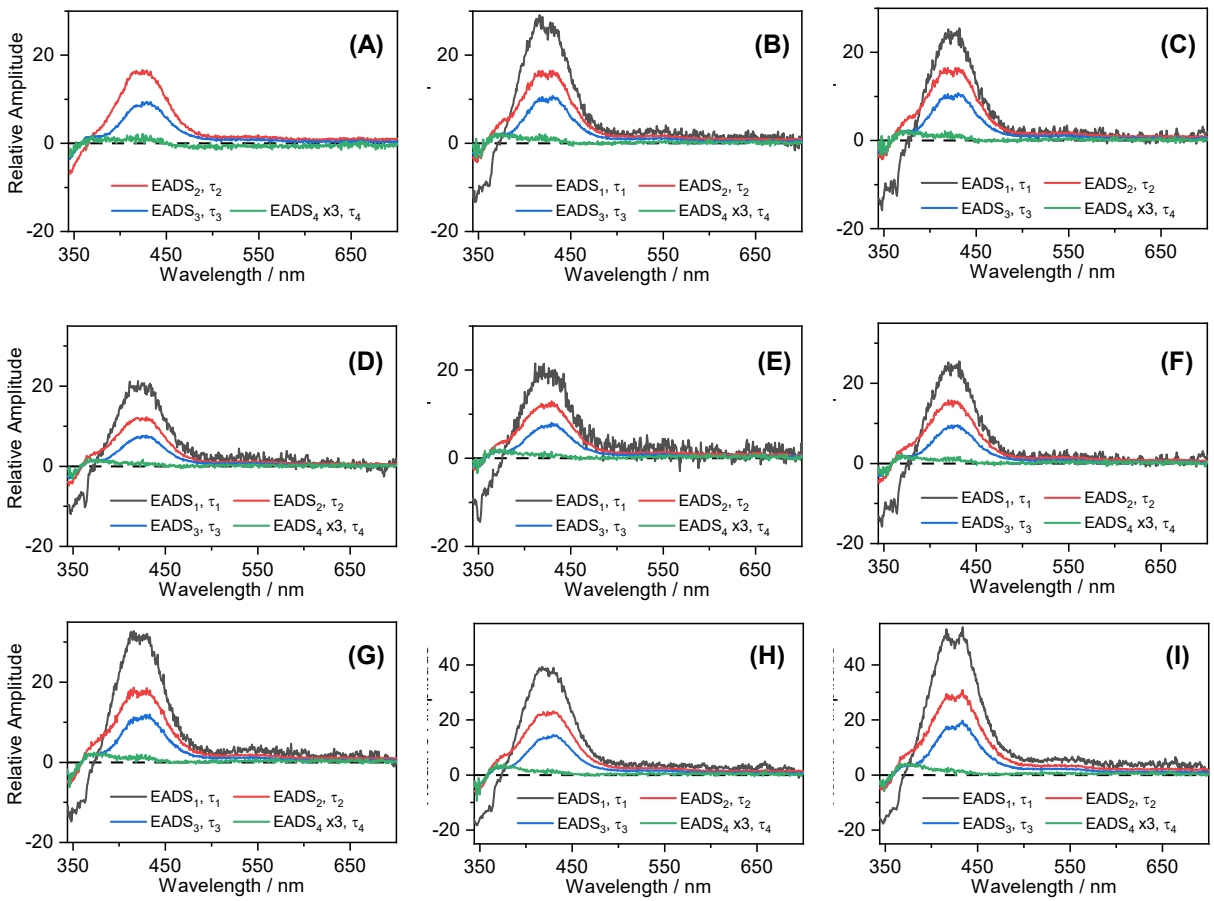

data for sinapoyl-L-malate and its derivatives

Figure S47: EADS extracted from the sequential global fitting of the transient spectra for (A) SM, (B) DESM, (C) DBSM (D) DOSM, (E) DLSM, (F) DCSM, (G) DGSM, (H) DFSM, and (I) DOleySM. In panel (A) EADS1 have been omitted due to the large error associated with it.

Residuals from the global fitting of transient data for sinapoyl-L-malate and its derivatives

The residuals from the sequential global fitting with respect to the raw transient electronic absorption (TEA) spectra data (*i.e.,* the difference between the fit and the raw data at each data point) are shown in Figure S46. The small-signal intensities of the residual compared to the raw TEA spectra shown in the main manuscript (Figure 4) demonstrate the quality of the fits.

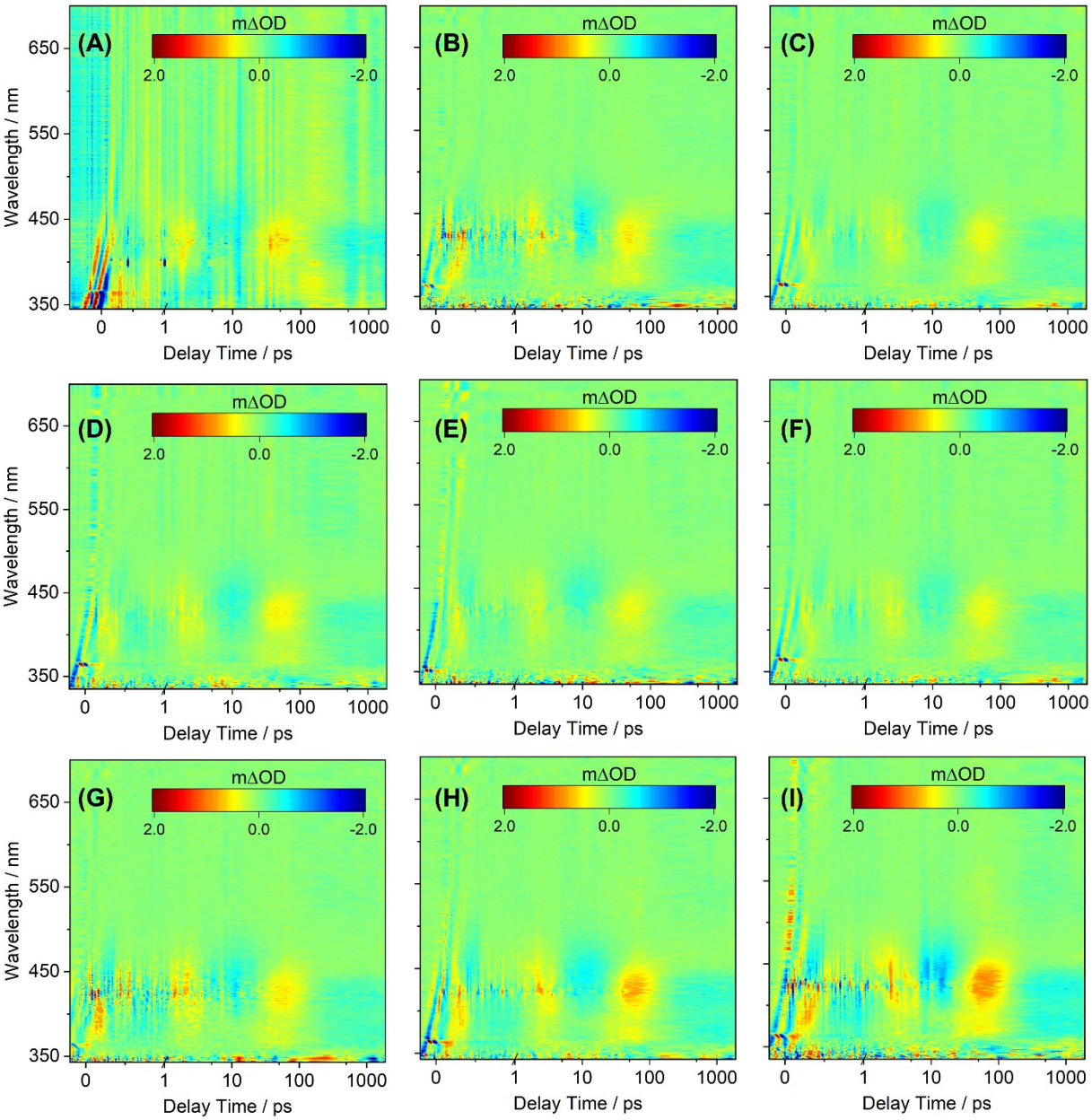

Figure S48: False colour heatmap for the residuals obtained from the sequential global fitting of the transient spectra for (A) SM, (B) DESM, (C) DBSM (D) DOSM, (E) DLSM, (F) DCSM, (G) DGSM, (H) DFSM, and (I) DOleySM.

Solvent alone instrument response

The TEAS measurements of the time zero solvent-only scan were recorded to obtain the instrument response function (IRF), which determines the limiting temporal resolution of the present transient experiments. The instrument response function in CCT photoexcited at 330 nm (Figure S47 (A)) has a strong contribution of cross-phase modulation between pump and probe pulses as they traverse our solvent medium. However, this should not affect the conclusions of the manuscript given the timescales we are investigating in the solute. For this reason, we chose to follow the approach of Kovalenko *et al.*[1], in which we use a frequency-dependent cross-correlation function to model the IRF in Figure S47 (B). The value obtained for the temporal resolution of the solvent-only time zero response is 120 fs.

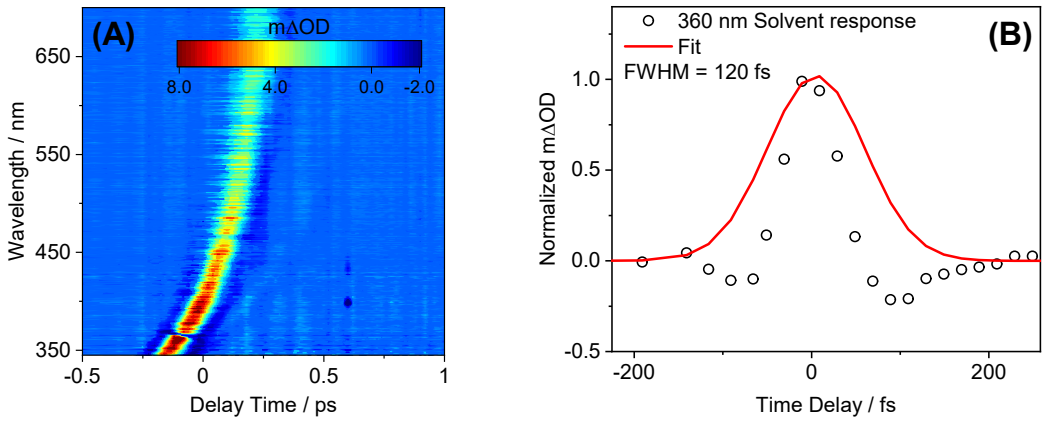

Figure S49: (A) False colour heatmap for CCT solvent only response. (B) Selected transients for solvent-only time-zero response at a probe wavelength of 360 nm with extracted full-width half maxima (FWHM) of 120 fs. This value is used as the instrument response in the global fit analysis of all the TEA spectra.

Reference

1 Kovalenko, S. A., Dobryakov, A. L., Ruthmann, J. & Ernsting, N. P. Femtosecond spectroscopy of condensed phases with chirped supercontinuum probing. *Physical Review A* **59**, 2369-2384, doi:https://doi.org/10.1103/PhysRevA.59.2369 (1999).